

Semi Centralized Training Decentralized Execution Architecture for Multi Agent Deep Reinforcement Learning in Traffic Signal Control

Pouria Yazdani^{a,1}, Arash Rezaali^{a,1} and Monireh Abdoos^{a,*}

^a*Faculty of Computer Science and Engineering, Shahid Beheshti University, Tehran, Iran*

ARTICLE INFO

Keywords:

Adaptive Traffic Signal Control
Region based Multi-Agent Deep Reinforcement Learning
Semi Centralized Training
Decentralized Execution

ABSTRACT

Multi-agent reinforcement learning (MARL) has emerged as a promising paradigm for adaptive traffic signal control (ATSC) of multiple intersections. Existing approaches typically follow either a fully centralized or a fully decentralized design. Fully centralized approaches suffer from the curse of dimensionality, and reliance on a single learning server, whereas purely decentralized approaches operate under severe partial observability and lack explicit coordination resulting in suboptimal performance. These limitations motivate region-based MARL, where the network is partitioned into smaller, tightly coupled intersections that form regions, and training is organized around these regions. This paper introduces a *Semi-Centralized Training, Decentralized Execution* (SEMI-CTDE) architecture for multi intersection ATSC. Within each region, SEMI-CTDE performs centralized training with regional parameter sharing and employs composite state and reward formulations that jointly encode local and regional information. The architecture is highly transferable across different policy backbones and state–reward instantiations. Building on this architecture, we implement two models with distinct design objectives. A multi-perspective experimental analysis of the two implemented SEMI-CTDE-based models covering ablations of the architecture’s core elements including rule based and fully decentralized baselines shows that they achieve consistently superior performance and remain effective across a wide range of traffic densities and distributions.

1. Introduction

Traffic congestion is a major and complex challenge for cities worldwide with the rapid growth of urbanization and vehicle ownership. Longer commute times, excessive fuel consumption, and elevated air pollution levels are direct consequences of over-saturated roads. For instance, according to the 2024 INRIX Global Traffic Scorecard, individual commuters in Istanbul, New York City, and Chicago experienced total annual delay of about 105, 102, and 102 hours, respectively, underscoring the magnitude of intersection-driven delays in major metros (INRIX). Within urban networks, signalized intersections are the dominant bottlenecks: the policies implemented at these intersections allocate scarce space–time among competing traffic streams and therefore largely determine corridor-level delay, queues, and emissions.

Reinforcement learning (RL) has become a standard practice for adaptive traffic signal control (ATSC), controlling phase selection and timing as a sequential decision problem that optimizes long-horizon objectives such as delay, throughput, and emissions under nonstationary demand (Yau et al., 2017). Deep RL (DRL) extends this by using function approximation to digest rich state representations—from detector queues to trajectories and graph-structured networks—enabling policies that generalize across varying traffic flows and topologies (Zhao et al., 2024). Collectively, this body of work motivates moving beyond single-intersection controllers toward coordinated, network-level solutions and setting the stage for multi-agent formulations.

Multi-agent deep reinforcement learning (MADRL) (Hu et al., 2024) is a natural fit for ATSC because intersections are inherently distributed decision makers whose actions jointly shape corridor and network dynamics. Modeling each intersection as an intelligent agent allows policies to adapt to local, nonstationary demand while learning coordination mechanisms that propagate benefits downstream—e.g., smoothing platoons and preventing spillback. By enabling jointly coordinated decisions among neighboring agents, MADRL captures the coupled structure of real networks more faithfully than Independent RL (IRL) formulations.

However, applying MARL to city traffic networks presents several key challenges. Traffic intersections do not operate independently: the queue discharge from one intersection becomes the inflow for downstream intersections, causing spatial–temporal dependencies across the network. If each agent optimizes signal timings in isolation, ignoring these couplings, it can lead to suboptimal or even adverse emergent behaviors (e.g., one intersection starving its neighbors or causing spillback). The multi-agent setting is inherently complex and partially observable from any single intersection’s perspective—each agent has a limited local view, and the environment’s dynamics become non-stationary as all agents learn concurrently. Ideally, a fully centralized controller would coordinate all intersections jointly, explicitly accounting for the state and flows of every other agent to optimize global performance (Casas, 2017); yet in practice it is computationally intractable at city scale due to huge joint state space and action space and imposes prohibitive latency and communication burdens (Chu et al., 2020). Conversely, a purely decentralized (independent) approach where each traffic light learns on its own lacks global optimality and may fail to resolve traffic network-level congestion patterns

*Corresponding authors.

E-mail address: m_abdoos@sbu.ac.ir (M. Abdoos).

¹Co-first authors. These authors contributed equally to this work.

(Bao et al., 2023). In summary, pure centralized and pure decentralized solutions each have shortcomings. This recognition has driven researchers towards hybrid approaches that balance coordination and scalability, namely distributed-training decentralized-execution frameworks, encompassing a spectrum of training paradigms that vary in their degree of centralization—from fully centralized to fully decentralized. (Noaen et al., 2022; Saadi et al., 2025).

Among these, region based multi-agent approaches have gained attention as a practical compromise between fully centralized and fully decentralized control. By partitioning a city network into smaller regions of closely interacting intersections, one can reduce complexity and improve coordination locally. Recent studies have shown that dividing a traffic network into strongly coupled regions (based on real-time flow densities) and solving regional sub-problems can significantly speed up learning and boost performance compared to tackling the entire city as one problem Li et al. (2024). Within this line of work, the co-design of state and reward is pivotal for region based multi-agent approaches because each intersection must reason along two complementary perspectives: a local context (e.g., approach-level queues) and a region context that abstracts coupled dynamics across same-region neighbors—a top-down view of directional imbalances, upstream/downstream pressures, and interface conditions at region boundaries.

Our research thoroughly investigates how a region-based MADRL architecture can operate effectively under this co-design while avoiding the drawbacks of fully centralized and fully decentralized training paradigms. We argue that partitioning the traffic network into tightly coupled regions of intersections and then applying centralized learning within each region using co-designed composite states that capture both local and regional information, paired with composite rewards that jointly optimize local throughput and regional coordination substantially enhances overall traffic efficiency in traffic networks. To make these ideas practical, we propose a structured architecture that generalizes across alternative instantiations, allowing regional based methods to be implemented with different policy backbones, communication strategies and state and reward definitions. We refer to this architecture as SEMI-CTDE : **S**emi-Centralized **T**raining, **D**ecentralized **E**xecution, which we primarily study in the context of urban traffic signal control.

This paper’s main contributions are summarized as follows:

- Structured, modular SEMI-CTDE architecture using MADRL. We propose a region-based SEMI-CTDE architecture for TSC that explicitly co-designs composite state and reward definitions together with their dedicated feature blocks, ensuring that both local and regional aspects of traffic dynamics are captured. The architecture is highly transferable, allowing different policy backbones, feature extraction methods, and

region formation algorithms to be substituted without changing the underlying conceptual design.

- Two realized implementations. We instantiate the proposed architecture in two models with distinct design objectives, providing concrete examples of how the SEMI-CTDE architecture can be applied in practice.
- Comprehensive and multi-perspective experiments. Core elements of the proposed architecture are assessed through targeted ablation studies and evaluations across diverse traffic conditions, yielding clear relationships between region partitioning, composite state/reward design and different design objectives under varying demand conditions.

2. Related Works

RL and MARL have seen widespread adoption in addressing ATSC problems in recent years, owing to their model-free formulation, strong empirical performance, and ability to adapt to diverse traffic conditions (Yau et al., 2017). The review in this section begins with RL methods designed for single-intersection environments and then transitions to multi-intersection networks, covering both centralized and distributed MARL schemes for ATSC; we further examine methods for extracting regions from urban traffic networks and survey region-based MARL frameworks proposed for adaptive traffic signal control.

2.1. Reinforcement Learning for Traffic Signal control

Early work on ATSC model a single intersection as a Markov decision process and applied tabular RL, most notably Q-learning (Watkins and Dayan, 1992), to learn mappings from compact state descriptors (e.g., current phase and approach queues) to discrete phase-change actions through trial and error (Abdulhai et al., 2003). While these methods demonstrated that RL can outperform fixed-time and actuated control in simulation, they relied on coarse state discretization, small action spaces, and carefully engineered features. As a result, they struggled to represent rich detector information, to generalize across operating conditions, and to scale gracefully as the number of phases, lanes, and movements grew (Noaen et al., 2022).

DRL approaches for single-intersection control address many of these limitations by learning value or policy approximators over higher-dimensional representations (Rasheed et al., 2020). (Liang et al., 2019) formulate the intersection as a grid-based state constructed from sensor data and use a dueling double-DQN with prioritized replay to adapt cycle lengths and phase durations, achieving lower delay and shorter queues than classical plans. (Ault et al., 2020) develop an interpretable DRL-based precedence-function controller and three DQN variants that tune a polynomial control function, showing that such a regulatable policy can match DNN-based controllers. These works illustrate how DRL can exploit richer state spaces with consistent reward

function formulations and more expressive policies than tabular RL. Lots of research and review has been done in this manner (Zhao et al., 2024; Saadi et al., 2025; Bouktif et al., 2023). While single-intersection RL controllers can improve local performance, real-world urban networks invariably include multiple interacting intersections whose dynamics are mutually dependent, making multi-agent RL formulations essential for capturing these dependencies and coordinating signal plans across the network.

2.2. Multi Agent Deep Reinforcement Learning

For multi-intersection adaptive control, the most direct extension of single-agent DRL is to treat the whole network as a single global agent, yielding a centralized-training centralized-execution (CTCE) architecture. In this setting a single deep network observes a global state that aggregates measurements from all intersections and outputs a joint action vector specifying the signal timings network-wide. A representative example is the spatio-temporal DRL model of (Yi et al., 2022), which encodes the entire network’s traffic conditions into a spatio-temporal feature representation and computes signal plans for all junctions within one centralized controller. Such CTCE schemes can in principle exploit global information to coordinate signals, but they quickly encounter the curse of dimensionality in both the state and action spaces as the network grows.

To improve scalability while retaining some form of centralized guidance, many recent works adopt a centralized-training-decentralized-execution (CTDE) paradigm, where each intersection is an agent with its own executable policy, but training is assisted by a centralized critic or server. One line of work employs global critics or value-decomposition structures: for example, (Bie et al., 2024) propose a collaborative MARL method with a spatio-temporal graph attention network and value decomposition to learn a joint value function over heterogeneous intersections while deploying decentralized policies at execution time; and (Song et al., 2024) use a counterfactual multi-agent actor-critic approach in which a centralized critic leverages joint observations to compute counterfactual advantages for each intersection actor. A second line introduces explicit parameter-server or federated mechanisms: (Ren et al., 2024) propose a two-layer coordinated RL scheme where local agents send experience to a central learner that optimizes a coordination policy and broadcasts updated parameters back to the intersections, while (Li et al., 2025) design a federated DRL framework in which intersection agents periodically upload locally trained models to a central server for aggregation and then receive a global model for continued training and decentralized execution. Other CTDE approaches emphasize neighborhood structure in the agent design: (Cai et al., 2025) models each intersection as an interpretable multi-agent RL controller that conditions on local and neighboring information, yet still relies on a central learner that aggregates experience across agents during training while policies are executed locally at each intersection.

A third family pursues fully decentralized training and execution (DTDE), where there is no central critic or server and both learning and control are carried out in a distributed manner. Early work by (Abdoos et al., 2011) applies independent multi-agent Q-learning, training a separate tabular Q-learner at each intersection using only local state and reward, without any explicit coordination mechanism. More recent methods introduce local cooperation via peer-to-peer communication or consensus: (Liu and Ding, 2022) propose a distributed DRL method in which each intersection trains a local deep controller and uses a consensus algorithm over the communication graph to align policies without a central learner; (Liu et al., 2025)’s decentralized neighboring information fusion (D-NIF) algorithm further develops this idea by letting agents fuse neighbors’ information and exchange parameters through an extra-gradient consensus step, achieving both decentralized modeling and decentralized distributed training; and (Wu et al., 2020) design a multi-agent DRL scheme for urban traffic light control in vehicular networks where controllers are deployed at intersections and coordinate via local information exchange within the communication network, again without a global training server. Together, these CTCE, CTDE, and DTDE intersection-level MARL schemes illustrate the spectrum from fully centralized to fully decentralized designs, and motivate region-level MARL architectures that seek a middle ground between global coordination and scalability.

2.3. Region-based MARL for TSC

Region-based MARL approaches extend these ideas by introducing an intermediate spatial scale: instead of controlling each intersection independently or aggregating the whole network into a single agent, the network is partitioned into regions of tightly coupled intersections and RL controllers are defined at the region level. The effectiveness of such schemes depends critically on how these regions are constructed. Beyond the RL literature, several works in traffic flow theory have studied how to partition heterogeneous networks into internally homogeneous, strongly interacting regions; for example (Saeedmanesh and Geroliminis, 2016) propose a clustering procedure that groups links into macroscopic-fundamental-diagram-consistent regions based on directional flow patterns, while (Xing et al., 2022) design a dynamic regional partitioning method for active traffic control that updates control subareas according to evolving congestion and correlation patterns. These ideas motivate the use of data-driven zoning as a basis for region-level reinforcement learning.

At the algorithmic level, one line of work keeps a largely centralized perspective and uses regions primarily as a decomposition of the global problem. The CODER framework of (Tan et al., 2020) partitions a large traffic grid into several subregions with identical topology, trains a DRL agent for each subregion, and then introduces a centralized global agent that aggregates regional value estimates into a single global Q -function from which the joint action over

all regions is selected. Training and execution therefore still pass through a global coordinator, and the region abstraction mainly serves to reduce the dimensionality and facilitate reuse of subregion policies rather than to fully decentralize control.

In contrast, region-level CTDE methods assign a distinct learning agent to each region and rely on centralized or shared components only during training. RegionSTLight (Li et al., 2024) derives a regional multi-agent Q-learning framework in which the global Q -value is decomposed into a sum of regional Q -values and combines this with a dynamic zoning scheme that groups intersections into strongly coupled regions on the basis of real-time link flow densities; a lightweight spatio-temporal fusion network encodes intra-region interactions, while the value-decomposition structure provides centralized guidance during training and execution remains distributed across regions. Building on this line of work, (Gu et al., 2025) augment regional MARL architectures such as RegionLight and Regional-DRL with GA2 communication modules that aggregate macro- and micro-level traffic states across regions; although control actions are issued by regional agents, parameter updates depend on globally aggregated information, preserving the CTDE character at the region scale.

Several region-level DTDE approaches push decentralization further by letting each region learn independently from its own experience. The fuzzy-graph-based method of (Abdoos, 2021) first extracts correlated sets of intersections as regions using an α -cut on a fuzzy relation graph and then learns a single Q-learning controller per region on regional states and rewards, without any global critic. Region-Light (Gu et al., 2024) formulates a constrained network-partitioning problem that produces star-topology regions and trains an adaptive deep RL controller in each region independently, while (Lu et al., 2025) employ a regional soft actor-critic scheme in a connected-vehicle environment where SAC agents control predefined regions using local and neighboring information. Together, these works show that region-based MARL can be realized along the same CTCE-CTDE-DTDE spectrum as intersection-level methods, while region formation and region-level state and reward design play a central role in balancing scalability, decentralization, and coordination.

Overall, the literature shows that, despite substantial progress, there is still no unified, region-centric MADRL architecture that cleanly balances coordination, scalability, and practical deployability for urban TSC. These gaps motivate us to develop and empirically test a SEMI-CTDE architecture that is explicitly region-centric, couples principled region formation with co-designed composite state and reward representations, and centralizes learning only within tightly coupled regions while preserving decentralized execution at the intersection level.

Table 1
Summary of key notations.

Notation	Description
I	Set of all intersections in the network
R_k	Region k
$R(i)$	Region to which intersection i belongs
K	Number of regions in the partition
U	Set of regional agents
U_k	Set of regional agents associated with region k
$u(i)$	Regional agent assigned to intersection i
π_ϵ	ϵ -greedy action-selection policy
θ	Parameters of the Q-network
\mathcal{A}^G	Global action space
\mathcal{A}_i	Admissible action set of intersection i
$a_i^{(n)}$	Action of intersection agent i at decision step n
$t_i^{(n)}$	Time of the n -th decision at intersection i
$g(a_i^{(n)})$	Green duration associated with action $a_i^{(n)}$
$c(a_i^{(n-1)}, a_i^{(n)})$	Inter-phase clearance from $a_i^{(n-1)}$ to $a_i^{(n)}$
S_i	State space of intersection i
$r_i^{(n)}$	Reward assigned to intersection i at decision step n
s_i^{local}	Local component of composite state at intersection i
s_i^{regional}	Regional component of composite state at intersection i
ϕ_i^{phase}	Local phase-context feature vector at intersection i
$\phi_i^{\text{throughput}}$	Local throughput feature vector at intersection i
ϕ_i^{spatial}	Local spatial/topological feature vector at intersection i
ψ_i^{phase}	Regional phase-context feature vector at intersection i
$\psi_i^{\text{throughput}}$	Regional throughput feature vector at intersection i
ψ_i^{spatial}	Regional spatial/topological feature vector at intersection i
$r_i^{\text{local}}(a_i^{(n)})$	Local reward term of intersection i at decision step n
$r_i^{\text{regional}}(a_i^{(n)})$	Regional reward term of intersection i at decision step n
$\rho_{R(i)}^{\text{local}}$	Weight on r_i^{local} in region $R(i)$
$\rho_{R(i)}^{\text{regional}}$	Weight on r_i^{regional} in region $R(i)$
D_{R_k}	Region-level shared replay memory for region R_k
θ_k	Parameters of the regional DDQN for region R_k
$\hat{\theta}_k$	Target-network parameters of the regional DDQN for region R_k
$Q_i(s, a)$	Global Q-values produced by regional agent u_i for state s and action a
done $_i$	Terminal flag for intersection agent i in replay tuples
phase $_i$	One-hot vector encoding current signal phase at intersection i
q_i^{vert}	Normalized halted-vehicle count on vertical through approaches at i
q_i^{hor}	Normalized halted-vehicle count on horizontal through approaches at i
$q_i^{\text{vert-left}}$	Normalized halted-vehicle count on vertical left-turn approaches at i
$q_i^{\text{hor-left}}$	Normalized halted-vehicle count on horizontal left-turn approaches at i
$\bar{q}_i(n)$	Topology-normalized sum of queue lengths over all approaches to i at decision step n
$\mathcal{E}_{R(i)}$	Set of all approaches belonging to region $R(i)$
τ	Spillback threshold for halted vehicles on an approach
$\mathcal{E}^{\text{boundary}}$	Set of boundary approaches of $R(i)$
N_i^{hop}	Ordered set of directional one-hop neighbors of intersection i
$\bar{q}_{R(i)}^{\text{mean}}(n)$	Region-averaged queue length over intersections in $R(i)$ at decision step n
$\sigma_{R(i)}(n)$	Fraction of intersections in $R(i)$ currently in a yellow phase at decision step n
Δt_j	Remaining time until neighbor j 's next decision step
N_i^{vert}	Number of advancing vehicles on vertical approaches to intersection i
N_i^{hor}	Number of advancing vehicles on horizontal approaches to intersection i
p_i^{vert}	Total number of vehicles on vertical approaches to intersection i
p_i^{hor}	Total number of vehicles on horizontal approaches to intersection i
\mathcal{V}	Set of completed vehicle trips in the simulation
w_v	Total waiting time of vehicle v
τ_v	Travel time of vehicle v

3. Problem Definition

In this section we outline RL-based modeling of TSC and then establish the problem formulation for region-based MARL in TSC. Key notations used throughout this paper are summarized in Table 1.

3.1. RL-based Modeling of Traffic Signal Control Problem

A natural way to see the problem of ATSC is to model each signalized intersection as a Markov Decision Process (MDP) that repeatedly maps observed traffic conditions into signal decisions. Formally, at each decision time t , an intersection i is represented as $(s_t, a_t, P, r_t, \gamma)$: the *state* $s_t \in \mathcal{S}$ summarizes local traffic sufficient to approximate the Markov property (Sutton and Barto, 2018); the *action* $a_t \in \mathcal{A}$ selects the next admissible signal operation (e.g., switch/hold/extend); the *transition kernel* $P(s_{t+1} \mid s_t, a_t)$ is determined by stochastic arrivals and network flow dynamics over the resulting control interval, so the inherent uncertainty in approaching traffic flows is acknowledged; and the *reward* $r_t = r(s_t, a_t)$ encodes operational objectives such as reducing delay and queues.

The control goal is to choose a *policy* $\pi(a \mid s)$ that maximizes the expected discounted return:

$$J(\pi) = \mathbb{E}_{\pi} \left[\sum_{t=0}^{\infty} \gamma^t r(s_t, a_t) \right], \quad \gamma \in (0, 1), \quad (1)$$

where the expectation is taken over trajectories generated by $s_{t+1} \sim P(\cdot \mid s_t, a_t)$ and $a_t \sim \pi(\cdot \mid s_t)$. Here, the discount factor γ geometrically down-weights future rewards, induces an effective horizon $H_{\text{eff}} \approx (1 - \gamma)^{-1}$, and (for $0 < \gamma < 1$) makes the Bellman operator a contraction. Choosing γ close to 1 emphasizes long-term congestion mitigation, whereas smaller γ prioritizes immediate delay reductions.

This formulation captures the core tension in TSC. Phase decisions at each step affect not only instantaneous delay but also future congestion through P and γ . Modeling each intersection as an MDP thus provides a principled foundation to reason about sequential trade-offs under uncertainty. In practice, formulating control as an MDP admits two broad solution strategies: *model-based* methods that plan by explicitly predicting how the system will evolve under candidate actions, and *model-free* methods that instead learn effective policies directly from experience without constructing an explicit dynamics model. In this work we adopt the latter, model-free approach.

Model-free Q-learning (Watkins and Dayan, 1992) operationalizes the objective (1) by learning the optimal action-value function $Q^*(s, a)$ without estimating the transition model P . Given the return $J(\pi)$ above, value functions satisfy the Bellman relations:

$$\begin{aligned} V^{\pi}(s) &= \mathbb{E}[r(s, a) + \gamma V^{\pi}(s') \mid s] \\ Q^{\pi}(s, a) &= \mathbb{E}[r(s, a) + \gamma \mathbb{E}_{a' \sim \pi(\cdot \mid s')} Q^{\pi}(s', a')] \end{aligned} \quad (2)$$

Here, $V^{\pi}(s)$ is the *state-value* under policy π , and $Q^{\pi}(s, a)$ is the *action-value*; $r(s, a)$ is the instantaneous or delayed reward obtained when the *agent* takes action a after observing state s ; s' denotes the *next observation/state*; and the nested expectation $\mathbb{E}_{a' \sim \pi(\cdot \mid s')}$ expresses that the next action is *chosen* according to policy π . The outer expectation is with respect to the stochastic transition $s' \sim P(\cdot \mid s, a)$. The optimal counterpart obeys the Bellman optimality equation:

$$Q^*(s, a) = \mathbb{E} \left[r(s, a) + \gamma \max_{a' \in \mathcal{A}} Q^*(s', a') \right]. \quad (3)$$

Q-learning updates a tabular estimate toward this fixed point using sampled transitions (s_t, a_t, r_t, s_{t+1}) :

$$\begin{aligned} Q_{t+1}(s_t, a_t) &\leftarrow Q_t(s_t, a_t) + \eta \delta_t \\ \delta_t &= r_t + \gamma \max_{a' \in \mathcal{A}} Q_t(s_{t+1}, a') - Q_t(s_t, a_t) \end{aligned} \quad (4)$$

where δ_t is the *temporal-difference (TD) error* between the target and current estimate; $\eta \in (0, 1]$ is the *learning rate*; and (s_t, a_t, r_t, s_{t+1}) are sampled by the agent while

interacting with the environment; action selection balances exploration and exploitation via an ϵ -greedy policy:

$$\pi_{\epsilon}(a \mid s) = (1 - \epsilon) \mathbb{I} \left\{ a = \arg \max_{a'} Q_t(s, a') \right\} + \frac{\epsilon}{|\mathcal{A}|}. \quad (5)$$

This *model-free, policy-learning* scheme directly yields a control law $\pi(s) = \arg \max_a Q_t(s, a)$ from experiences, but a tabular Q scales as $\mathcal{O}(|S||\mathcal{A}|)$ and cannot generalize across large, continuous, or high-dimensional descriptions of traffic states—typical in TSC.

Deep Q-learning (DQN) (Mnih et al., 2015) addresses this by approximating $Q(s, a)$ with a neural network $Q_{\theta}(s, a)$ and minimizing a temporal-difference regression loss over mini-batches drawn from an experience replay memory \mathcal{D} :

$$\begin{aligned} \mathcal{L}(\theta) &= \mathbb{E}_{(s, a, r, s') \sim \mathcal{D}} \left[(y - Q_{\theta}(s, a))^2 \right] \\ y &= r + \gamma \max_{a' \in \mathcal{A}} Q_{\bar{\theta}}(s', a') \end{aligned} \quad (6)$$

Here, Q_{θ} , represents the Q network, is a *trainable* parametric approximator whose weights θ are updated via stochastic gradient steps to minimize $\mathcal{L}(\theta)$; \mathcal{D} stores past *experiences* to decorrelate samples; $\mathcal{L}(\theta)$ is the mean-squared TD loss; $Q_{\bar{\theta}}$ is a slowly updated *target network*—a lagged copy of Q_{θ} —used solely to compute the bootstrapped target y ; the *online network* Q_{θ} produces the prediction being trained. In practice, its parameters are copied from the online network at fixed intervals ($\bar{\theta} \leftarrow \theta$ every C training steps). Finally, y is the one-step TD *target* computed from the next observation s' using this fixed snapshot $Q_{\bar{\theta}}$.

To reduce the overestimation bias of the max operator, *Double DQN (DDQN)* (van Hasselt et al., 2016) decouples action selection and evaluation in the target:

$$y_{\text{DDQN}} = r + \gamma Q_{\bar{\theta}} \left(s', \arg \max_{a' \in \mathcal{A}} Q_{\theta}(s', a') \right). \quad (7)$$

In this target, the next action is selected by the online network Q_{θ} but evaluated by the target network $Q_{\bar{\theta}}$, which mitigates positive bias while preserving the model-free nature of control.

With these components—function approximation for scalability, replay memory for decorrelation, and target networks (plus DDQN) for bias/variance control—(Rasheed et al., 2020) value-based DRL retains the experience-driven, model-free character of Q-learning while making it practical for the rich state representations encountered in traffic signal control.

3.2. Region-based MARL for Traffic Signal Control

We model urban traffic signal control as a multi-agent decision process in which multiple intersections act concurrently and are organized into spatial regions that capture tightly coupled behavior. Here we provide this formulation to fix

the core entities, notation, and performance criteria that will carry through the rest of the paper.

Regional Agent. In our formulation we distinguish the learning module from the physical signal controller. A *regional agent* refers to the decision-making model parameterized by a DDQN, as introduced in §3.1. This DDQN represents a policy that maps an observed state to action values. In other words, the agent is the learner: it is the function approximator that is optimized during training and later queried at runtime.

Intersection Agent. An *intersection agent* is an individual signalized intersection that executes control within the traffic environment. At each control step, the intersection agent observes its own traffic conditions, encodes them as a state vector, and queries the DDQN policy associated with it to obtain and perform the next admissible signal operation. Intersection agents are heterogeneous. To better reflect real urban networks, we include both four-leg (cross) intersections and three-leg (T) intersections with its variants (Figure 1); these geometries admit different non-conflicting movements and therefore expose different admissible actions. This geometric structure also influences which features are present in their state representation when it queries a regional agent. As a result, multiple distinct intersection agents (with different layouts and feasible phase sets) can be served by the same regional agent, while still behaving in a coordinated yet localized manner.

Region. A *region* \mathcal{R} is a set of intersection agents whose behaviors are strongly coupled: queues, spillback, and discharge at one intersection agent can immediately influence its neighbors. In practice, such regions can be derived from high-density corridors, spatial adjacency, or any structural pattern that creates tight mutual dependence. A region is treated as a coordination unit during training, while execution at runtime remains intersection-level. We denote by $\mathcal{R}(i)$ the (unique) region to which intersection agent i belongs. The entire traffic network is partitioned into K disjoint regions $\{\mathcal{R}_1, \dots, \mathcal{R}_K\}$:

$$I = \bigcup_{k=1}^K \mathcal{R}_k, \quad \mathcal{R}_j \cap \mathcal{R}_\ell = \emptyset \text{ for } j \neq \ell$$

Here, I denotes the set of all intersection agents in the network.

Let U denote the set of regional agents. Each region \mathcal{R}_k is associated with a nonempty regional agent set $U_k \subseteq U$, with $|U_k| \geq 1$ (e.g., a single shared agent or multiple/hierarchical regional agents). At runtime, each intersection agent $i \in \mathcal{R}_k$ queries a designated regional agent $u(i) \in U_k$ for control, where u_i denotes the regional agent assigned to coordinate control for intersection i within region K . The general problem formulation in this setting is depicted in Figure 2.

Action Space. At each decision step n , the intersection agent at intersection i issues an action $a_i^{(n)}$ that selects which signal phase logic to activate and for how long it will remain active.

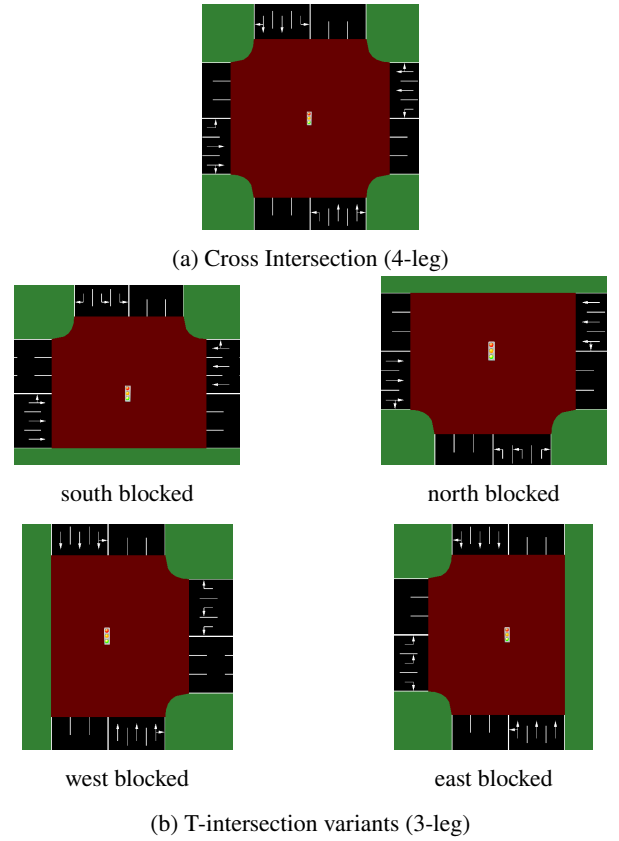


Figure 1: Representative intersection topologies considered. (a) 4-leg Cross Intersection with all approaches present. (b) 3-leg T-Intersections in multiple geometric configurations. Different geometries imply different conflict-free movement phases and thus different admissible action sets for each intersection agent.

For a standard four-leg (cross) intersection, we define four admissible phase logics: NS_S (north–south through movements only), NS_L (north–south protected left turns), EW_S (east–west through movements only), and EW_L (east–west protected left turns). Each logic can be executed with one of two discrete duration options: a *short* phase of g_s seconds or a *long* phase of g_l seconds. This yields eight concrete actions (NS_S short, NS_S long, NS_L short, NS_L long, EW_S short, EW_S long, EW_L short, EW_L long) that the policy may select at runtime. The inclusion of multiple duration choices allows the controller to modulate service intensity without assuming a fixed control interval, making the action space closer to realistic actuated signal practice.

When switching between different phase logics (e.g., from NS_S to EW_L), a mandatory yellow/all-red clearance of 3 s is enforced for safety; transitions that simply continue the same logic at a different duration do not require an intermediate clearance. For T-intersections, which lack one approach of the crossroads, the action space \mathcal{A}_i is defined as the feasible subset of these same phase logics. In other words, each intersection agent’s admissible action set \mathcal{A}_i is intersection agent-specific and physically valid by construction. We formally define \mathcal{A}^G as the global action

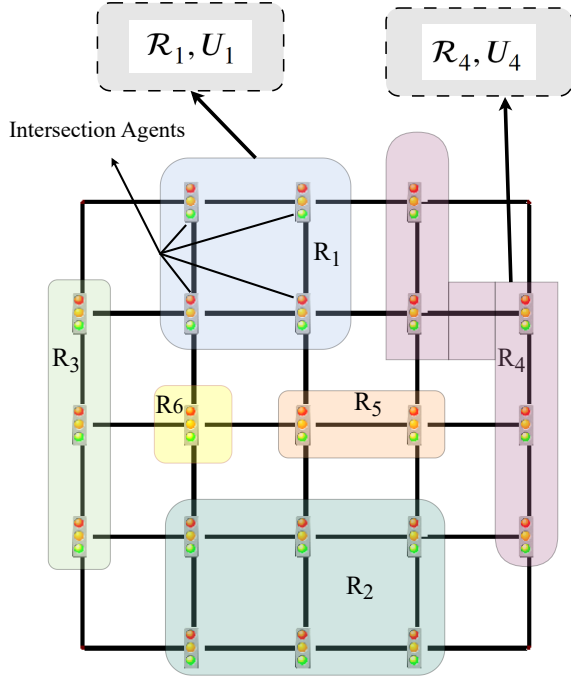


Figure 2: Region based MARL for TSC

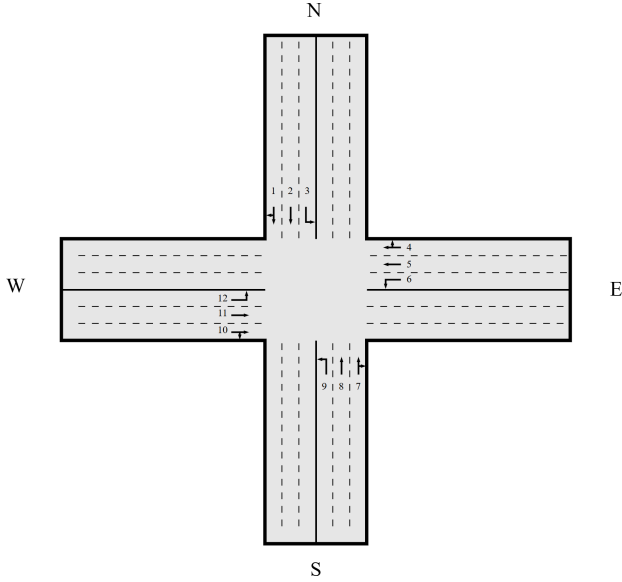


Figure 3: Base geometry and lane indices used to define phase logics at a standard 4-leg intersection (cf. Table 2).

space and, for each intersection i , let $\mathcal{A}_i \subseteq \mathcal{A}^G$ denote its admissible (topology-valid) action set. Figure 3 depicts the base geometry and lane indices for a standard four-leg intersection, and Table 2 summarizes the global action space \mathcal{A}^G .

Because each phase logic admits two duration options, we adopt an event-driven schedule: after issuing action $a_i(t_i^{(n)})$, the next decision occurs when the executed green expires plus any required inter-phase clearance. Where $n \in$

Table 2

Concurrent lane service under each phase logic at a standard 4-leg intersection \mathcal{A}^G . Each row lists the lane groups (by ID) that receive green simultaneously.

Phase logic	Served lanes
NS_S short, NS_S long	1, 2, 7, 8
NS_L short, NS_L long	1, 3, 7, 9
EW_S short, EW_S long	4, 5, 10, 11
EW_L short, EW_L long	4, 6, 10, 12

\mathbb{N} indexes the decision steps at intersection i . Formally,

$$t_i^{(n+1)} = t_i^{(n)} + g(a_i^{(n)}) + c(a_i^{(n-1)}, a_i^{(n)}). \quad (8)$$

where $g(\cdot)$ denotes the selected green duration and $c(\cdot, \cdot)$ encodes the yellow/all-red clearance when switching phase logic (zero when the logic is unchanged).

State. At each decision time t , intersection agent i aggregates its observable operating context into a fixed-length state vector $s_i^{(t)} \in S_i \subseteq \mathbb{R}^d$, where S_i denotes the state space. This vector is a compact collection of informative traffic-flow features around intersection i . The state $s_i^{(t)}$ is then provided to the designated regional agent for $\mathcal{R}(i)$, which evaluates the admissible actions in \mathcal{A}_i and returns a control decision. During learning, these states serve as the inputs on which the region’s regional agent set is optimized to favor actions that improve long-term network performance.

Reward. At each decision time $t_i^{(n)}$, we attribute to intersection agent i a scalar reward $r_i(t_i^{(n)}) \in \mathbb{R}$ that evaluates the performance delivered at and around i . Because the effects of a signal change take effect with latency, this evaluation is computed after a fixed delay and assigned back to the decision taken at t . The signal is defined over the intersection agent’s operating context. Without committing to a specific shaping, $r_i(t_i^{(n)})$ should be read as an aggregation aligned with congestion mitigation and efficient discharge. The designated regional agent for $\mathcal{R}(i)$ uses these delayed rewards along with the observed states and chosen actions to improve decision making for long-horizon performance.

4. Approach: Semi-Centralized Training, Decentralized Execution

In this section we detail our proposed SEMI-CTDE architecture for ATSC.

4.1. Region Formation

In the context of optimizing traffic signal control, the formation of regions serves as a critical strategy to enable effective coordination among intersection agents. The primary goal of region formation is to optimize traffic flow by grouping intersections that exhibit strong mutual dependence in their traffic dynamics. This approach is particularly valuable for managing the interdependencies between tightly coupled intersections, where congestion, queues, and spillback at one

intersection can significantly affect its neighbors. Without coordinated control, these spatial and temporal interdependencies can result in suboptimal management, leading to increased delays and inefficiencies in traffic flow. By grouping intersections with similar traffic dynamics, regions isolate subsets of intersections that need to coordinate their control policies.

We adopt the *alpha-cut method* in fuzzy graphs, as proposed in (Abdoos, 2021), to partition the network. The traffic network is modeled as a fuzzy graph, where each vertex represents an intersection and edges reflect dependencies based on traffic flow and congestion. The alpha-cut method partitions the graph into regions by selecting a threshold α that defines the strength of interdependence between intersections. The resulting regions, or “correlated agent sets,” consist of intersections that are tightly coupled in terms of traffic dynamics, ensuring that coordination occurs primarily within these regions.

In SEMI-CTDE, regional agents oversee the behavior of intersection agents within their respective regions, so defining regions with these characteristics aligns naturally with this architecture. By facilitating coordinated actions within these regions, SEMI-CTDE built on meaningful region formation improves traffic management and helps to minimize delays. Intersection agents acting together within a region can more effectively mitigate congestion and prevent spillbacks, leading to better overall system performance compared to controlling the entire traffic network as a single entity.

4.2. State Space Design

In MADRL based traffic signal control, state representation is crucial since the chosen action at each decision step is highly dependent on the perceived information from the local and regional environment. In order to better address the details in state space design, SEMI-CTDE requires each intersection agent i to expose composite s_i to its regional agent. We conceptualize s_i as a modular concatenation

$$s_i = [s_i^{\text{local}} \parallel s_i^{\text{regional}}], \quad (9)$$

Let $s_i \in \mathbb{R}^d$ with $s_i^{\text{local}} \in \mathbb{R}^{d_\ell}$ and $s_i^{\text{regional}} \in \mathbb{R}^{d_r}$, where $d = d_\ell + d_r$ and \parallel denotes concatenation.

where the local component captures intersection-specific operating context and the regional component summarizes the surrounding coordination context within i ’s region. Because execution and querying are decentralized, SEMI-CTDE tolerates richer state representations per intersection agent while retaining coordinated learning benefits via shared regional training.

In SEMI-CTDE, both components are instantiated as structured feature vectors each with fixed goal. We organize the local state of intersection agent i as

$$s_i^{\text{local}} = [\psi_i^{\text{phase}} \parallel \phi_i^{\text{throughput}} \parallel \phi_i^{\text{spatial}}] \quad (10)$$

Algorithm 1 Region Formation via Fuzzy Graph α -Cut

```

1► Inputs: Intersection set  $\mathcal{I}$ ; simulation horizon  $n$ ; threshold  $\alpha$ .
2► Initialization: Define directed graph  $G = (V, E)$  with  $V \leftarrow \mathcal{I}$ ,  $E \leftarrow \emptyset$ .
   Warm-up phase: collect congestion data
3► for  $t = 1$  to  $n$  do
4►   for all intersection  $i \in \mathcal{I}$  do
5►     Update cumulative queues on incoming edges of  $i$ .
6►   end for
7► end for
8► for all intersection  $i \in \mathcal{I}$  do
9►    $\text{queue}(i) \leftarrow$  average queue length on incoming edges of  $i$ .
10► end for
   Graph construction: assign congestion weights to edges
11► for all intersection  $i \in \mathcal{I}$  do
12►   for all downstream intersection  $j$  reachable from  $i$  do
13►     Add  $(i, j)$  to  $E$  with weight  $c_{ij} \leftarrow \text{queue}(i)$ .
14►   end for
15► end for
   Fuzzy memberships
16► for all vertex  $v \in V$  do
17►    $\sigma(v) \leftarrow$  avg congestion on incoming edges of  $v$ .
18► end for
19► for all edge  $(u, v) \in E$  do
20►    $p_{uv} \leftarrow \frac{c(u,v)}{\sum_j c(j,v)}$ .
21►    $\mu(u, v) \leftarrow \min(\sigma(u), \sigma(v)) \cdot p_{uv}$ .
22► end for
   Apply  $\alpha$ -cut on edges
23► for all edge  $(u, v) \in E$  do
24►   if  $\mu(u, v) < \alpha$  then
25►     Remove edge  $(u, v)$  from  $E$ .
26►   end if
27► end for
   Region extraction
28► Construct undirected graph  $G_\alpha$  from  $G$  by keeping only edges with  $\mu(u, v) \geq \alpha$ .
29► Perform connected component analysis on  $G_\alpha$ .
30► Output: Regions  $\{\mathcal{R}_1, \dots, \mathcal{R}_K\}$ , where each  $\mathcal{R}_k$  is a connected group of intersections.

```

where the three sub-vectors respectively encode phase context, throughput features, and spatial/topological features at intersection agent i . In parallel, we recommend constructing the regional component as

$$s_i^{\text{regional}} = [\psi_i^{\text{phase}} \parallel \psi_i^{\text{throughput}} \parallel \psi_i^{\text{spatial}}] \quad (11)$$

so that the final designed state space aggregates region-level information that is aligned with the local-state representation.

This modular construction makes explicit how SEMI-CTDE decomposes each state component, while leaving the exact feature choices within each block to the practitioner and the specifics of the deployment traffic network.

Local State s_i^{local} : The local state is limited to intersection agent i and its immediate approaches, encoding only information that can be measured from its own incoming/outgoing movements and fixed topological properties. Its role is to describe how well i is currently operating or

has operated in the very recent past and what structural constraints shape feasible control patterns, without relying on any explicit region-level aggregation. Accordingly, as in (10), we instantiate s_i^{local} using three main features.

Local Phase Context ϕ_i^{phase} : This feature characterizes the current control strategy at intersection agent i , providing the agent with short-term operational memory of how the signal is behaving. Typical elements include the current action or active phase, an indicator of whether the intersection is in an intermediate state such as a yellow transition, and the number or rate of recent logical phase switches over a short horizon. These features help the agent reason about phase continuity, switching penalties and existence of stop-and-go behavior when selecting the next action.

Local Throughput Features $\phi_i^{\text{throughput}}$: This feature summarizes how effectively intersection i is processing vehicles on its immediate approaches. It may include lane- or approach-level queue lengths, average speeds, cumulative or mean waiting times, local demand or arrival rates, and simple discharge or outflow measures on the incoming and outgoing links. By exposing both congestion indicators and throughput measures, this component allows the policy to directly target reduced delay, controlled queue growth, and efficient utilization of green time at the local scale.

Local Spatial/Topological Features ϕ_i^{spatial} : This feature encodes invariant structural properties of intersection i that shape its role in the network. Examples include whether intersection i is a T or cross intersection, its connectivity pattern such as direction of incoming approaches with respect to itself, and a role indicator such as perimeter vs. interior intersection in grid-like networks. Such features enable the learned policy to associate consistent behaviors with similar geometric and topological roles, improving generalization across heterogeneous intersections while preserving a uniform local-state encoding.

Regional State s_i^{regional} : The regional component equips the intersection agent with a top-down view that extends beyond intersection i 's immediate incoming approaches and summarizes how its surrounding intersections in region $\mathcal{R}(i)$ are operating. The exact same goals in Local State s_i^{local} are followed here and the distinction is in the scope of the encoded features. A key design choice is the receptive field: one may use (a) whole-region summaries that pool information over all intersection agents in $\mathcal{R}(i)$ to expose global imbalances and overall loading, or (b) bounded-neighborhood summaries that emphasize the most influential vicinity to sharpen local coordination; either option is compatible with SEMI-CTDE, and the choice should reflect region size and complexity of learning network in terms of number of learnable parameters. To convert a large number of regional features into a fixed-length representation, one can employ invariant pooling (e.g., sum/mean/max over sets) or directionally organized summaries to encode directional imbalance where appropriate, with region size anchoring the trade-off between expressivity and dimension.

Regional Phase Context ψ_i^{phase} : The same principles as the local feature counterpart apply, but extended to characterize the coordination environment around i . Instead of only the current phase of a single intersection, this feature encodes aggregated or neighborhood-level information about active phases, recent switching behavior, or synchronization patterns within $\mathcal{R}(i)$. This enables the agent to infer whether it operates within a predominantly compatible, conflicting, or desynchronized regional signal configuration when selecting its next action.

Regional Throughput Features $\psi_i^{\text{throughput}}$: Analogously to the local throughput feature, this regional throughput summarizes congestion and discharge indicators at the regional scale, constructed via the receptive field choices outlined above. It aggregates quantities such as regional queue burdens, delays, or utilization over $\mathcal{R}(i)$, while preserving a fixed-size encoding. In addition, SEMI-CTDE recommends explicitly incorporating throughput indicators at region boundaries (e.g., inflow/outflow at perimeter approaches), so that the regional signal captures how well the region exchanges traffic with its surroundings and where coordinated discharge is most needed.

Regional Spatial/Topological Features ψ_i^{spatial} : Following the same design logic as the local spatial feature, the regional counterpart encodes structural information at the regional scale in a way that remains portable across alternative partitions. Typical elements include the relative position of intersection i within $\mathcal{R}(i)$, descriptors of the region's layout, and explicit boundary indicators for nodes or approaches adjacent to other regions. These features allow the policy to associate distinct coordination behaviors with different regional roles and to learn about cross-region interactions.

When instantiating concrete features within each of local and regional components, it is recommended to ensure that both local and regional components expose signals closely aligned with the evaluation objectives (e.g., delay reduction, throughput, spillback avoidance), so that improvements in the learned policy translate directly into gains in the chosen performance metrics; second, It is advised to maintain scale-comparable encodings that normalize number of approaches for each intersection and region size, so that shared policies remain comparable across intersections and regions of different topologies and size. In combination, the resulting block-structured state design yields a compact, interpretable, and well-organized representation that separates local detail from regional context, supports decentralized execution at individual intersections, and still permits effectively centralized learning within each region through shared regional agents that consume a consistent, semantically coherent state space.

4.3. Reward Function Design

In traffic-signal control, the general network-level objective is to minimize average travel time across the network. Because this global performance signal is neither directly

observable at decision time nor immediately attributable to individual control actions, reward formulations instead rely on measurable quantities that approximate or correlate with travel time. Under SEMI-CTDE, each intersection agent i , between two consecutive decision times $[t_i^{(n)}, t_i^{(n+1)})$, receives a composite reward attributed to the action taken at $t_i^{(n)}$:

$$r_i(t_i^{(n)}) = \rho_{\mathcal{R}(i)}^{loc} r_i^{local}(t_i^{(n)}) + \rho_{\mathcal{R}(i)}^{reg} r_i^{regional}(t_i^{(n)}). \quad (12)$$

Here, the local term evaluates traffic flow quality at intersection i , and the regional term captures coordination effects within region $\mathcal{R}(i)$. The weights $(\rho_{\mathcal{R}(i)}^{loc}, \rho_{\mathcal{R}(i)}^{reg})$ are defined per region and determine the tradeoff between local and regional objectives. These weights are kept constant to promote training stability and are chosen empirically. These two terms should be designed with careful attention to several practical considerations; we summarize the key guidelines below.

Local reward $r_i^{local}(t_i^{(n)})$: At each decision step, this term assesses the quality of traffic flow performance at intersection i by prioritizing observable reductions in vehicle delay and containment of queue growth, thereby promoting sustained discharge and spillback avoidance. To keep comparisons fair across heterogeneous geometries (e.g., three-leg versus four-leg layouts), contributing quantities should be normalized with respect to physical geometry so that comparable operational performance yields comparable reward irrespective of topology. The features used should be co-designed with the local state vector in 4.2, drawing on the same congestion and flow factors so that what the agent perceives is tightly aligned with what it is incentivized to improve, strengthening feedback assignment and sample efficiency. To mitigate stop-and-go behavior at intersections, it is also helpful to penalize frequent phase switches which could introduce lost time and inefficiencies. A design including some or all these elements can better approximate the general travel time objective.

Regional reward $r_i^{regional}(t_i^{(n)})$: By contrast to the local term, this component evaluates performance across the entire region $\mathcal{R}(i)$ that contains intersection i , encouraging coordination that addresses shared bottlenecks and improves region-boundary throughput. It should retain the same core design principles as the local term but lifted to the regional scale: favoring region-level delay and queue mitigation; geometry-based normalization to remain geometry- and size-agnostic so that regions with different numbers of approaches or intersections are comparable; consideration of the regional state vector in 4.2 to achieve consistency; and penalizing frequent phase switches. For the regional reward term, like receptive field choice in regional state design, two principled and complementary options are advisable: whole-region summaries that pool information over neighborhood intersection agents in $\mathcal{R}(i)$ to expose global imbalances and overall loading, and bounded-neighborhood summaries that emphasize the most influential vicinity to sharpen local coordination. Either option is compatible with SEMI-CTDE,

and the selection should reflect region size, topology, and corridor structure.

Overall, the composite reward in (12) provides action-attributable feedback that jointly reflects local and regional coordination objectives, thereby supporting consistent reward assignment under the decentralized execution paradigm of SEMI-CTDE, while the use of region-specific weights (ρ_{loc}, ρ_{reg}) further allows each region to calibrate the trade-off between local performance and regional coordination to its own topology and demand pattern without sacrificing the consistency of the overall architecture.

4.4. Proposed Architecture (SEMI-CTDE)

Given a fixed partition of the network into regions (cf. 4.1), we now describe how the *Semi-Centralized Training, Decentralized Execution* paradigm operates over these regions. Fig. 4 depicts the proposed architecture of SEMI-CTDE inside each region.

4.4.1. Instantiation of Region Entities

Let $\{\mathcal{R}_1, \dots, \mathcal{R}_K\}$ denote disjoint regions over the set of intersection agents I (cf. 3.2). Each region \mathcal{R}_k is served by a *single* regional agent a_k parameterized by a DDQN. Thus, $U_k = \{u_k\}$, and every intersection agent $i \in \mathcal{R}_k$ maps to $u(i) = u_k$ for control. Intersection agents differ in geometry and feasible phase sets but share the same regional agent within \mathcal{R}_k . The network partition employed throughout this work—obtained using the procedure of 4.1—is illustrated in Fig. 5.

4.4.2. Intersection Agent-Side Processing Modules

Each intersection agent i contains two *independent, non-trainable* processing units that operate before and after querying its regional agent. These units depend on the agent’s geometry and its location within the region—but do not depend on the regional agent or its parameters. We refer to them as the *Topology & Location Encoder (TLE)* and the *Action Mapping Module (AMM)*.

(1) **Topology & Location Encoder (TLE)** — before query. At each $t_i^{(n)}$, intersection agent i deterministically encodes observations into a topology- and location-aware state vector $s_i^{enc}(t_i^{(n)})$ using a routine that depends only on the intersection agent’s physical type and its placement within the region, and is independent of the regional agent, thereby making encodings region-comparable without altering dimensionality. The TLE’s responsibility is orthogonal to the concrete state definition: regardless of which features are chosen, location and topology always induce intersection agent-specific canonicalization; the TLE is where these effects are resolved so the regional agent always receives a region-comparable, fixed-layout encoding. Formally, for each intersection agent i let TLE_i : denote the deterministic encoder; at each decision

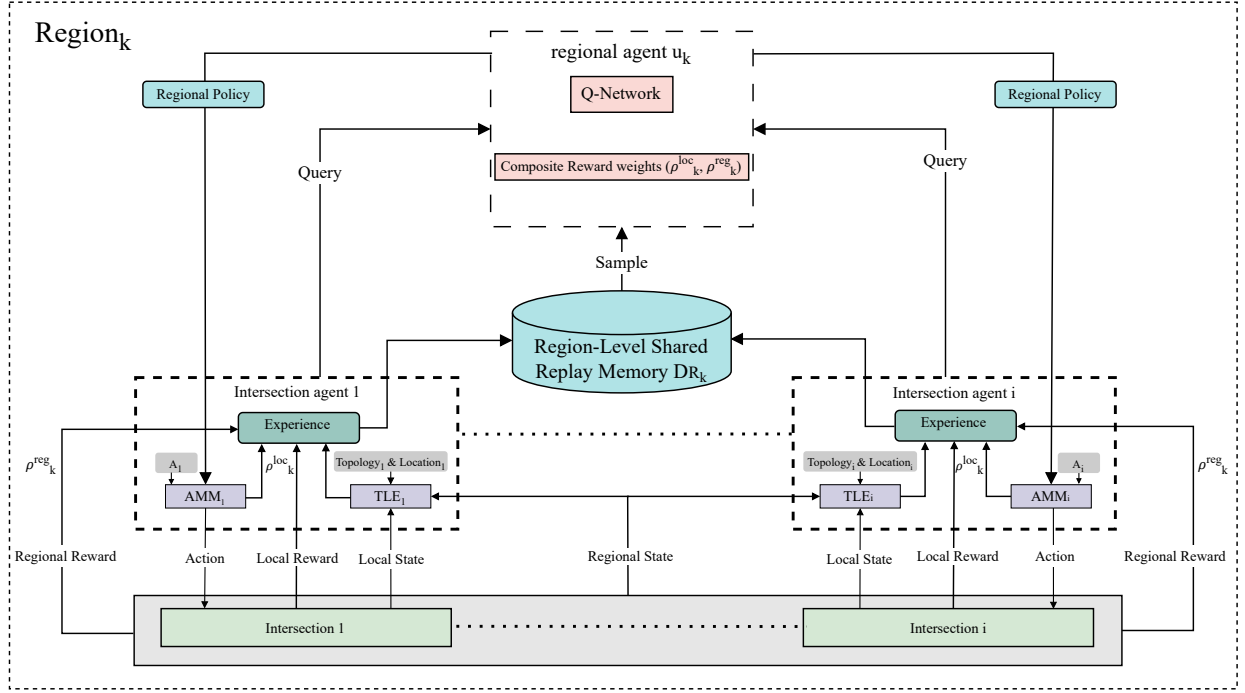


Figure 4: SEMI-CTDE architecture inside each region.

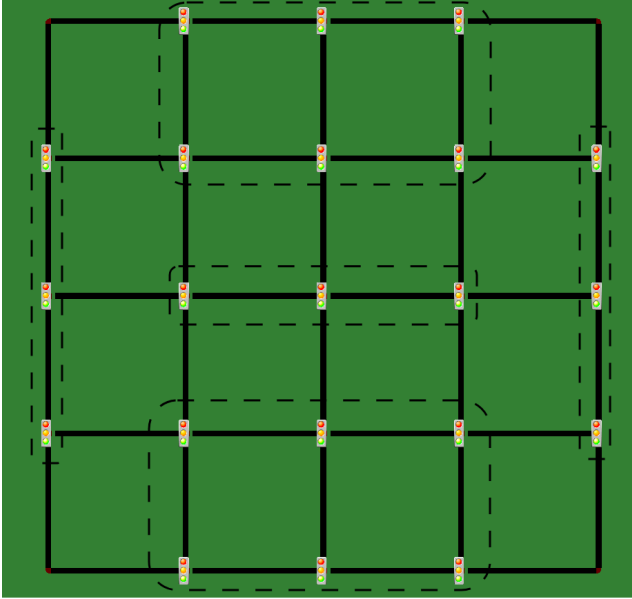


Figure 5: Network partition into regions $\{\mathcal{R}_k\}_{k=1}^K$ used in this paper. Traffic lights denote intersection agents; dashed lines mark region boundaries. The partition is obtained via the method described in 4.1.

step,

$$s_i^{\text{enc}}(t_i^{(n)}) = \text{TLE}_i(s_i(t_i^{(n)})) \quad (13)$$

(2) Action Mapping Module (AMM) — after query. Upon receiving the global Q vector from the regional agent, the

AMM deterministically reconciles these scores with the intersection agent’s heterogeneous, geometry-specific action space. It applies a fixed, topology-aware mapping from the global action space \mathcal{A}^G to the intersection agent’s admissible set \mathcal{A}_i , discarding ineligible entries so selection (and any exploration) occurs only over valid actions. Crucially, when writing the transition to the regional replay memory, the AMM stores the intersection-valid, actually executed Q value corresponding to the selected admissible action after mapping. This module is rule-based and independent of the regional agent; its role is to enforce physical validity and preserve correct action semantics in both decision-making and experience gathering. Formally, for each intersection agent i define a deterministic mapping AMM_i . At each decision step:

$$Q_i(t_i^{(n)}) = \text{AMM}_i(Q_{\theta_k}(s_i^{\text{enc}}(t_i^{(n)}), \cdot)) \in \mathcal{A}_i, \quad (14)$$

and for any index $a \in \mathcal{A}_i$ selected from this vector, the action is executed directly according to \mathcal{A}_i ’s local phase semantics.

Together, TLE (before-query) and AMM (after-query) let heterogeneous, intersection agents expose consistent states to a shared regional agent and execute physically valid controls from global Q values. This design preserves decentralized execution while enabling semi-centralized learning under shared regional parameterization.

4.4.3. Intersection Agents and the Regional Agent

Within each region \mathcal{R}_k , the regional agent u_k serves as a shared global controller for all intersection agents $i \in \mathcal{R}_k$. The regional agent is a single DDQN with parameters θ_k and $\bar{\theta}_k$ and a region-level replay memory D_{R_k} . Intersection agents act as local controllers: they (i) acquire raw sensor signals locally, (ii) run the TLE to produce a fixed-layout, region-comparable state, (iii) query u_k for Q -values, and (iv) invoke their AMM to reconcile the global Q with their topology-specific action set \mathcal{A}_i , issue the control signal, and store the intersection agent-valid, actually executed value in the experience written to D_{R_k} .

4.4.4. Asynchronous experience gathering and querying

Intersections agents start an episode synchronously but diverge as soon as they commit to different phase logic durations, so decision step timing becomes intersection agent-specific and query times are therefore generally nonaligned. Within each region, each intersection agent queries u_k at intervals determined by Eq. (8), yielding generally distinct query times. Each intersection agent closes its preceding transition by observing the delayed reward attributable to $a_i^{(n)}$ and forming (s, a, r, s') . This event-driven mechanism accumulates experiences asynchronously yet maintains correct temporal feedback assignment, since rewards are attached to the action that occupied the green until its scheduled decision step.

4.4.5. Regional Optimization and Parameter Sharing

Within each region \mathcal{R}_k , a single regional agent a_k maintains one parameter vector θ_k shared by all intersection agents in \mathcal{R}_k . Experiences generated asynchronously by the intersection agents are written to the region-level shared replay memory D_{R_k} , from which updates to θ_k are performed—realizing semi-centralized training at region scope while preserving decentralized execution at the intersections. Parameter sharing fosters within-region consistency in value estimation and action preferences, and the inclusion of all intersection agents' experiences in D_{R_k} further promotes coordinated behavior by exposing the regional agent to heterogeneous geometries, traffic conditions, and decision timing patterns within the same region.

4.4.6. Execution-Time Decentralization

After training, each intersection agent $i \in \mathcal{R}_k$ acts locally by forming s_i^{enc} , querying the frozen regional agent a_k and performing the inferred control signal. No inter-region communication is required at runtime; coordination arises from regional parameter sharing during training and the state/reward alignment.

4.4.7. Instantiation Degrees of Freedom

SEMI-CTDE does not prescribe low-level training mechanics. Beyond the state space (4.2) and reward function (4.3) backbones, several interfaces are intentionally left open

Algorithm 2 SEMI-CTDE

```

1► Inputs: Region partition  $\{\mathcal{R}_k\}_{k=1}^K$ ; global action space  $\mathcal{A}$ ;
   reward weights  $(\rho_{\mathcal{R}(i)}^{\text{loc}}, \rho_{\mathcal{R}(i)}^{\text{reg}})$ ; green-duration function
    $g(\cdot)$ ; clearance time  $c(\cdot, \cdot)$ ; exploration policy  $\Pi_{\text{explore}}$ ;
   training-step trigger  $\mathcal{T}_{\text{step}}$ ; target network update law  $\mathcal{L}_{\text{target}}$ ;
   minibatch sampler  $\mathcal{B}_k : (D_{R_k}, |\mathcal{B}|)$ ; per-intersection agent
   TLE $i$ ; per-intersection agent AMM $i$ .
2► Initialization: For each region  $k$ : initialize regional agent
   parameters  $\theta_k, \bar{\theta}_k$  and shared replay  $D_{R_k}$ .
3► for episode = 1 to  $M$  do
4►   reset environment;  $t \leftarrow 0$ 
5►   while episode not terminal do ▷  $x$ 
6►     for all regions  $k = 1, \dots, K$  do
7►       for all intersection agents  $i \in \mathcal{R}_k$  with  $t = t_i^{(n)}$  do
8►         State build: form  $s_i$  using (9)
9►         TLE: gather  $s_i^{\text{enc}}(t_i^{(n)})$  using (13)
10►        AMM: extract  $Q_i(t)$  from  $u_k$  using (14)
11►        Action selection:  $a_i^{(n)} \leftarrow \Pi_{\text{explore}}(Q_i(t))$ .
12►        Actuation & scheduling: perform  $a_i^{(n)}$  and
           schedule next query using (8).
13►      end for
14►    end for
15►    advance simulation step to the next event time
            $t \leftarrow \min_i t_i^{(n+1)}$ .
16►    for all regions  $k = 1, \dots, K$  do
17►      for all intersections  $i \in \mathcal{R}_k$  with  $t = t_i^{(n+1)}$  do
18►        observe next raw  $s_i(t)$  and set  $s_i^{\text{enc}} \leftarrow$ 
           TLE $i$  $(s_i(t))$ .
19►        Rewards: compute  $r_i(t_i^{(n)})$  using (12)
20►        Replay append: push
            $(s_i^{\text{enc}}(t_i^{(n)}), a_i^{(n)}, r_i(t_i^{(n)}), s_i^{\text{enc}}, \text{done}_i;)$ 
           to  $D_{R_k}$ .
21►      end for
22►      if  $\mathcal{T}_{\text{step}}$  triggers for region  $k$  at time  $t$  then
23►        sample minibatch  $\mathcal{B}$  according to  $\mathcal{B}_k$ 
24►        update  $\theta_k$  using  $\mathcal{B}$ .
25►        if  $\mathcal{L}_{\text{target}}$  triggers for region  $k$  then
26►           $\bar{\theta}_k \leftarrow \mathcal{L}_{\text{target}}(\theta_k, \bar{\theta}_k)$ 
27►        end if
28►      end if
29►    end for
30►  end while
31► end for

```

to implementation choice: the *target update rule* that governs synchronization between evaluation and target networks; the *exploration policy* that converts admissible value estimates into behavior; the *replay memory architecture* that specifies how experiences are stored and kept at region scope; and the *batch construction policy* that determines how samples are drawn for learning steps. Keeping these degrees of freedom explicit makes the architecture broadly applicable, easy to port across learning algorithms, and well suited to systematic ablations without altering the backbone.

5. Applying SEMI-CTDE: Two Implementations

In this section, we instantiate SEMI-CTDE with two concrete models that strictly follow the guidelines laid out in §4.2 and §4.3. Both implementations adopt the same region partitioning, regional agent architecture, and interaction mechanics described in §4.4; they differ only in how the regional components of the state and reward are constructed.

We refer to these two models as *RegionWide* and *OneHop*. Their distinction stems from the choice of receptive field used in the regional state and reward: OneHop employs a bounded neighborhood-based receptive field, whereas RegionWide uses whole-region summaries. We first define the local state and reward used in the OneHop and RegionWide models and instantiate the AMM employed in them. We then detail the regional state and reward formulations specific to each model.

5.1. Local State and Reward Definitions

Here we detail the identical local state and reward formulations employed in The OneHop and RegionWide models.

5.1.1. Local State s_i^{local}

Consistent with the s_i^{local} definition in Eq. (10), we instantiate the local state of intersection agent i as the concatenation of $\phi_i^{\text{throughput}}$, ϕ_i^{phase} and ϕ_i^{spatial} .

ϕ_i^{phase} : To encode the current control strategy, We use current signal phase at i represented by a one-hot vector

$$\phi_i^{\text{phase}} = \text{phase}_i \in \{0, 1\}^{\mathcal{A}^G}. \quad (15)$$

where $|\mathcal{A}^G| = 8$ (see table 2).

$\phi_i^{\text{throughput}}$: To measure how effectively intersection i is managing vehicles in immediate approaches, We group aggregating queue lengths caused by halted vehicles on incoming approaches into four scalars: q_i^{vert} , q_i^{hor} , $q_i^{\text{vert-left}}$ and $q_i^{\text{hor-left}}$.

denoting, respectively, the number of halted vehicles on vertical through approaches, horizontal through approaches, and their associated left-turn lanes. These quantities are normalized over the immediate incoming approaches and left-turn lanes according to the intersection topology. We collect them as

$$\phi_i^{\text{throughput}} = [q_i^{\text{vert}}, q_i^{\text{hor}}, q_i^{\text{vert-left}}, q_i^{\text{hor-left}}]. \quad (16)$$

We separate left-turn halted vehicles from their corresponding straight through movements to better align the state representation with the action space, where protected left-turn phases are controlled independently.

ϕ_i^{spatial} : To encode structural property of intersections, we use a 5-dimensional one-hot vector

$$\phi_i^{\text{spatial}} = \begin{cases} [1, 0, 0, 0, 0] & \text{west blocked,} \\ [0, 1, 0, 0, 0] & \text{east blocked,} \\ [0, 0, 1, 0, 0] & \text{south blocked,} \\ [0, 0, 0, 1, 0] & \text{north blocked,} \\ [0, 0, 0, 0, 1] & \text{4-way,} \end{cases} \quad (17)$$

indicating whether intersection i is one of the four T-intersection variants or a 4-way intersection.

5.1.2. Local Reward r_i^{local}

Consistent with the design principles in §4.3, we instantiate the local reward at intersection i as an average queue-length penalty over its immediate incoming approaches. Let $\bar{q}_i(n)$ denote the topology-normalized sum of queue lengths over all immediate approaches to intersection i at decision step n . We define local reward at decision time $t_i^{(n)}$ as

$$r_i^{\text{local}}(t_i^{(n)}) = -\bar{q}_i(n), \quad (18)$$

This choice directly penalizes congestion at intersection i by assigning more negative rewards when more vehicles are halted. By reusing exactly the queue lengths features that define $\phi_i^{\text{throughput}}$, this reward remains tightly aligned with what the agent perceives locally: actions that discharge queues and prevent spillback immediately reduce queue lengths at i and hence yield less negative local rewards.

5.2. AMM Instantiation

We instantiate the Action Mapping Module in both models using a topology-aware masking mechanism inspired by the admissibility masking mechanism proposed in (Wang et al., 2024).

At each decision time $t_i^{(n)}$, the regional agent produces a global Q -value vector over the full action space \mathcal{A}^G . The AMM then applies an elementwise mask over this vector, setting the entries corresponding to actions not admissible in \mathcal{A}_i to $-\infty$:

$$\text{AMM}_i(Q_{\theta_k}(s_i^{\text{enc}}(t_i^{(n)}), \cdot)) = \begin{cases} Q_{\theta_k}(s_i^{\text{enc}}(t_i^{(n)}), a), & a \in \mathcal{A}_i, \\ -\infty, & a \notin \mathcal{A}_i, \end{cases} \quad (19)$$

This masking step guarantees that the subsequent $\arg \max$ (or ϵ -greedy exploration) is performed strictly over the admissible subset \mathcal{A}_i , because all invalid actions are effectively removed from consideration.

5.3. RegionWide model

RegionWide employs whole-region summaries receptive field to encode regional information. This scheme is presented in Figure 6.

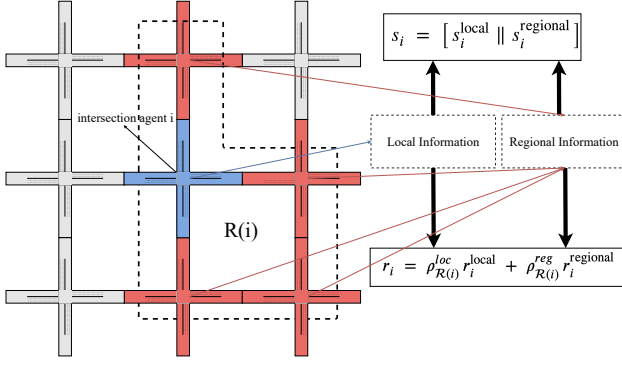


Figure 6: RegionWide model receptive field.

RegionWide Regional State s_i^{regional} : In the RegionWide model, each intersection agent i exposes to its regional agent a whole-region summary that aggregates information across all intersections within $\mathcal{R}(i)$. Consistent with the structured decomposition of s_i^{regional} in Eq. (11) we instantiate the regional features as follows.

ψ_i^{phase} : To represent the region-level phase configuration, we compute the proportion of intersections in $\mathcal{R}(i)$ currently executing each admissible phase logic in the global action set \mathcal{A}^G . Since \mathcal{A}^G contains four admissible phase logics, in this setup we obtain a four-dimensional vector

$$\psi_i^{\text{phase}} = \frac{1}{|\mathcal{R}(i)|} \left[\sum_{j \in \mathcal{R}(i)} \mathbf{1}\{\text{phase}_j = a_k\} \right]_{k=1}^4. \quad (20)$$

where a_1, \dots, a_4 enumerate the admissible phase logics. This feature exposes the regional distribution of active phases, allowing the regional agent to infer global synchronization patterns within the region.

$\psi_i^{\text{throughput}}$: The throughput block consists of three components capturing congestion, spillback, and regional exchange flows.

(i) We mirror the throughput structure used in the local state by incorporating the neighbor's halted-vehicle aggregates normalized according to j 's topology. We aggregate these quantities across $\mathcal{R}(i)$ using regional averaging:

$$\bar{q}_{\mathcal{R}(i)} = \frac{1}{|\mathcal{R}(i)|} \sum_{j \in \mathcal{R}(i)} [q_j^{\text{vert}}, q_j^{\text{hor}}, q_j^{\text{vert-left}}, q_j^{\text{hor-left}}]. \quad (21)$$

(ii) Let each approach in the region have halted vehicles q_a , and let the spillback threshold be $\tau = 15$, determined from approach length and width and vehicle size. The spillback ratio is

$$\chi_{\mathcal{R}(i)} = \frac{\sum_{a \in \mathcal{E}_{\mathcal{R}(i)}} \mathbf{1}\{q_a > \tau\}}{|\mathcal{E}_{\mathcal{R}(i)}|}, \quad (22)$$

representing the fraction of approaches experiencing severe congestion.

(iii) Let $\mathcal{E}_{\mathcal{R}(i)}^{\text{boundary}}$ denote the set of boundary approaches, i.e., approaches whose upstream and downstream intersections belong to different regions. For each such approach a , let ΔN_a denote the change in the number of vehicles present between two consecutive regional state update intervals. Over an update duration of length Δt , we compute

$$f_{\mathcal{R}(i)} = \frac{\sum_{a \in \mathcal{E}_{\mathcal{R}(i)}^{\text{boundary}}} \Delta N_a}{\Delta t}, \quad (23)$$

which provides a coarse estimate of the region's net exchange flow with its surroundings.

Collecting these three components yields the throughput feature:

$$\psi_i^{\text{throughput}} = [\bar{q}_{\mathcal{R}(i)}, \chi_{\mathcal{R}(i)}, f_{\mathcal{R}(i)}].$$

ψ_i^{spatial} : To encode the relative placement of intersection i within its region, we use a four-dimensional binary vector that indicates, for each cardinal direction, whether the corresponding one-hop neighbor lies outside $\mathcal{R}(i)$. Using $\mathcal{N}_i^{\text{hop}}$ to denote the directional neighbor set, we define ψ_i^{spatial} to denote the directional neighbor set, we define

$$\psi_i^{\text{spatial}} = [\mathbf{1}\{j \notin \mathcal{R}(i)\}]_{j \in \mathcal{N}_i^{\text{hop}}}, \quad (24)$$

where the neighbors in $\mathcal{N}_i^{\text{hop}}$ are ordered. This indicator identifies the boundary directions of intersection i and provides coarse spatial information useful for regional coordination.

Here the TLE determines which approaches are boundary approaches for computing $f_{\mathcal{R}(i)}$ and identifies which directional neighbors of intersection i lie outside $\mathcal{R}(i)$ when forming ψ_i^{spatial} . These topology- and location-derived indicators are resolved deterministically by the TLE so that s_i^{regional} remains region-comparable across heterogeneous intersections.

RegionWide Regional Reward r_i^{regional} : In the RegionWide model, the regional reward is constructed from whole-region congestion and flow indicators aligned with the regional state design. We first form a region-averaged queue

$$\bar{q}_{\mathcal{R}(i)}^{\text{mean}}(n) = \frac{1}{|\mathcal{R}(i)|} \sum_{j \in \mathcal{R}(i)} \bar{q}_j(n). \quad (25)$$

Next, we reuse the regional spillback ratio $\chi_{\mathcal{R}(i)}(n)$ and the boundary-flow indicator $f_{\mathcal{R}(i)}(n)$ introduced in the RegionWide state definition, and introduce a lost-time proxy $\sigma_{\mathcal{R}(i)}(n)$ defined as the fraction of intersections in $\mathcal{R}(i)$ that are currently in a yellow phase. The scalar regional reward associated with region $\mathcal{R}(i)$ at decision step n is then

$$\begin{aligned} r_i^{\text{regional}}(t_i^{(n)}) = & -\bar{q}_{\mathcal{R}(i)}^{\text{mean}}(n) \\ & -\lambda_{\text{spill}} \chi_{\mathcal{R}(i)}(n) \\ & -\lambda_{\text{switch}} \sigma_{\mathcal{R}(i)}(n) \\ & +\lambda_{\text{out}} f_{\mathcal{R}(i)}(n), \end{aligned} \quad (26)$$

which combines with $r_i^{\text{local}}(t_i^{(n)})$ to finalize the composite reward attributed to intersection i at decision step n .

To stabilize learning, the spillback, switching, and out-flow terms are smoothed over time using an exponential moving average, while the mean-queue term is kept unsmoothed to preserve its instantaneous sensitivity to congestion.

The regional coefficients λ_{spill} , λ_{switch} , and λ_{out} are tuned using Simultaneous Perturbation Stochastic Approximation (SPSA), a gradient-free stochastic optimization method that estimates the gradient of a noisy performance objective by randomly perturbing all parameters at once and forming a two-sided finite-difference estimate (Spall, 1992). In our setting, the objective is defined as the long-run performance of the learned policies under stochastic traffic demand and simulation noise. We first train the regional agents in an initial, long training block, and then proceed through a sequence of alternating short training and SPSA blocks. In each SPSA block, the learning procedure is completely frozen and for every region we generate two perturbed versions of its current coefficients in opposite directions and run paired probe episodes. The difference between the resulting regional rewards under these two oppositely perturbed coefficient settings provides a noisy gradient signal, which is then used to update the underlying coefficients in a direction that improves the average regional reward per episode. This interleaved schedule gradually adapts the regional reward weights while the policies themselves continue to train. Across tested configurations, the most effective balance between local and regional terms was obtained with $\rho_{\mathcal{R}(i)}^{\text{loc}} = 0.5$ and $\rho_{\mathcal{R}(i)}^{\text{reg}} = 0.5$ for all regions.

5.4. OneHop Model

OneHop uses bounded neighborhood receptive field to encode regional information. This scheme is presented in Figure 7.

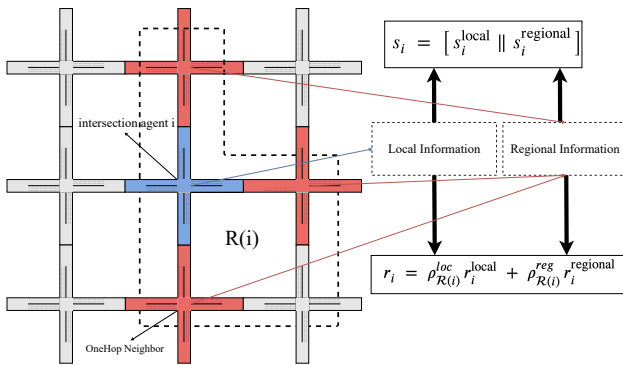


Figure 7: OneHop model receptive field.

OneHop Regional State s_i^{regional} : In this model, each intersection agent i exposes to its regional agent a short-range description of traffic conditions at and immediately around

itself. Rather than aggregating the entire region, the OneHop design focuses exclusively on i and its one-hop neighbors within the same region, enabling the regional agent to coordinate fine-grained interactions driven by local congestion propagation. Consistent with the structured decomposition of s_i^{regional} in Eq. (11) we instantiate the regional features as follows.

ψ_i^{phase} : For each one-hop neighbor $j \in \mathcal{N}_i^{\text{hop}}$ that lies in the same region as i , we include the neighbor's current signal phase encoded by the one-hot vector $\text{phase}_j \in \{0, 1\}^{|\mathcal{A}^G|}$, together with a scalar Δt_j giving the remaining time until j 's next decision step.

$$\psi_i^{\text{phase}} = [\{\text{phase}_j, \Delta t_j\}_{j \in \mathcal{N}_i^{\text{hop}}}] \quad (27)$$

$\psi_i^{\text{throughput}}$: First, we define vertical and horizontal approaching flows to i as

$$N_i^{\text{vert}} = p_i^{\text{vert}} - q_i^{\text{vert}} \quad N_i^{\text{hor}} = p_i^{\text{hor}} - q_i^{\text{hor}} \quad (28)$$

where p_i and q_i respectively denote the number of vehicles present and the number of vehicles halted on the immediate incoming approaches to intersection i , measuring how many vehicles are currently advancing toward i from its neighbors. Additionally, for each neighbor j , we further mirror the throughput structure used in the local state by incorporating the neighbor's halted-vehicle aggregates normalized according to j 's topology.

$$\psi_i^{\text{throughput}} = [N_i^{\text{hor}}, N_i^{\text{vert}}, q_j^{\text{vert}}, q_j^{\text{hor}}, q_j^{\text{vert-left}}, q_j^{\text{hor-left}}] \quad (29)$$

ψ_i^{spatial} : For each one-hop neighbor we consider the structural property using the same one-hot topology encoding defined for the local spatial feature in Eq. (17).

Collecting these elements over all neighbors in $\mathcal{N}_i^{\text{hop}}$, we obtain a fixed-layout representation even when the number of neighbors differs. Any neighbor that does not exist or lies outside the region partition is handled by the TLE, which inserts an all-zero placeholder for that neighbor's phase, throughput, and spatial blocks. This guarantees that the regional agent always receives a region-comparable, topology-consistent encoding of s_i^{regional} .

OneHop Regional Reward r_i^{regional} : In the OneHop model, the regional reward complements the local regional term by evaluating congestion in the immediate neighborhood surrounding intersection i . Consistent with the short-range regional state design, we define the regional reward as the negative aggregate queue of all one-hop neighbors of i that lie within the same region. Following the same notations

introduced in 5.1.2 the regional reward attributed to i at decision step $t_i^{(n)}$ is

$$r_i^{\text{regional}}(t_i^{(n)}) = - \sum_{j \in \mathcal{N}_i^{\text{hop}}} \bar{q}_j(n). \quad (30)$$

This formulation encourages intersection i to select actions that support local–neighbor coordination, relieving spillback pressure and stabilizing queue propagation across the immediate vicinity. The composite coefficients $(\rho_{\mathcal{R}(i)}^{\text{loc}}, \rho_{\mathcal{R}(i)}^{\text{reg}})$ balancing the local and regional components are determined empirically; in all experiments, the best-performing configuration was found to be $\rho_{\mathcal{R}(i)}^{\text{loc}} = 0.7$ and $\rho_{\mathcal{R}(i)}^{\text{reg}} = 0.3$ for all regions.

6. Experiments

This section details simulation setup, training details, experimental design and extensive comparison addressing the effect of SEMI-CTDE model design and its ablations. We then report quantitative results and discuss their implications.

6.1. General Settings

Here, we describe the common simulation and training configuration that underpins all experiments.

6.1.1. Traffic Network setting

In this paper we have used the well-known open source Simulation of Urban MObility (SUMO) simulator (Lopez et al., 2018), to conduct our experiments.

All models are trained and evaluated on a single 5×5 grid network with 25 intersections, of which 21 are signalized. All approaches have uniform length (470 m), and each approach provides three lanes. Lane-level turning permissions and right-of-way rules follow the specification in 3.2. The network comprises 9 cross-intersections and 12 T-intersections. A single vehicle class is used, with SUMO’s default speedFactor of 1.0 for all vehicles. Additionally, g_l and g_s are set to 15s and 5s respectively.

6.1.2. Traffic Flows

The distribution of vehicle arrival times determines the traffic demand injected into the network. During training, we use a uniform arrival distribution to stabilize learning, since real-world flows often exhibit peaks that corrupt convergence. For testing, we evaluate Weibull and Gaussian arrival distributions. The simulation horizon is fixed at 18,000 s. Table 3 summarizes the configuration of all flows used in this work.

6.1.3. Training setting

The training settings are identical across all models. All of them employ Double DQNs with a three-layer MLP

Table 3

Traffic flow configurations.

Distribution	Total vehicles (veh)	Avg. rate (veh/s)	Name
Uniform	39,600	2.2	U1
Gaussian	10,800	0.60	G1
Gaussian	13,500	0.75	G2
Weibull	14,400	0.60	W1
Weibull	10,800	0.70	W2
Weibull	18,000	1.0	W3
Weibull	19,800	1.1	W4

Table 4

Training details and hyperparameters.

Variable	Description	Value
ϵ_{\min}	Minimum exploration rate	0.01
ϵ_{decay}	Exploration decay	0.99
η	Learning rate	2.5×10^{-4}
γ	Discount factor	0.95
$ B $	Minibatch size	64
C_{policy}	Policy network update counter	20
C_{target}	Target network update counter	2000
$ D $	Replay memory capacity	5×10^4
\mathcal{O}	Optimizer	Adam
\mathcal{L}	Loss function	MSE

backbone (hidden sizes 512–256–128) between the input and output layers. Experiences are stored in a fixed-capacity replay memory with first-in–first-out replacement: once the buffer is full, newly collected transitions overwrite the oldest ones, so each experience remains available only for a limited number of episodes. Minibatches are sampled uniformly from the buffer, and exploration follows an ϵ -greedy policy with linear decay. Training details and hyperparameters are listed in Table 4.

6.1.4. Performance Evaluation Indicators

We assess model performance using four network-wide metrics computed over and during the full simulation horizon. Let \mathcal{V} denote the set of completed trips (vehicles that entered and exited the network), $|\mathcal{V}|$ their count, \mathcal{I} the set of signalized intersections, and $\{t_k\}_{k=1}^K$ the discrete time samples.

Average Waiting Time (AWT): Waiting time for vehicle v is the total time under a near-standstill threshold $v_{\text{th}} = 0.1$ m/s. Formally, letting w_v be total waiting time of vehicle v , We have

$$\text{AWT} = \frac{1}{|\mathcal{V}|} \sum_{v \in \mathcal{V}} w_v \quad (31)$$

Average Travel Time (ATT): Travel time for vehicle v is the elapsed time between its network entry and exit:

$$\tau_v = t_v^{\text{exit}} - t_v^{\text{entry}}, \quad \text{ATT} = \frac{1}{|\mathcal{V}|} \sum_{v \in \mathcal{V}} \tau_v \quad (32)$$

Average Queue Length (AQL): Let $q_i^{tot}(t_k)$ be the sum of queue lengths observed at all approaching lanes of intersection $i \in \mathcal{I}$ at time t_k . For network average we have

$$\text{AQL} = \frac{1}{|\mathcal{I}|K} \sum_{k=1}^K \sum_{i \in \mathcal{I}} q_i^{tot}(t_k) \quad (33)$$

6.2. Comparative Settings

In order to thoroughly verify the effectiveness of models designed under SEMI-CTDE, We compare them with other TSC algorithms as below.

6.2.1. Rule-based control methods

Actuated (ACT) : As a conventional traffic-responsive rule-based baseline, we employ the built-in actuated traffic signal controller provided by SUMO. This controller implements a detector-based, gap-out strategy: each phase is subject to a minimum green time, may be extended while upstream detectors register continuous demand, and is terminated once a critical gap elapses or the maximum green time is reached.

6.2.2. Fully decentralized

This baseline follows a purely decentralized learning paradigm with no region definition, communication, or parameter sharing. Each intersection i is controlled by an independent DDQN that optimizes its own signal policy using only locally observable information.

To isolate the value of SEMI-CTDE, we reuse the local components of our implementations of SEMI-CTDE, namely OneHop and RegionWide and remove all regional terms. Concretely,

$$s_i = s_i^{\text{local}}, \quad r_i = r_i^{\text{local}}. \quad (34)$$

This fully decentralized baseline represents a strong, commonly used reference in multi-agent TSC: it preserves sample efficiency and stability characteristics of DDQN while foregoing any explicit coordination. Performance differences relative to SEMI-CTDE models therefore quantify the incremental benefit of region definition and parameter sharing.

6.2.3. Partially SEMI-CTDE

This baseline is designed in order to address the effectiveness of composite state and reward definition and particularly regional components. This model implements all the guidelines of SEMI-CTDE including parameter sharing except the regional counterparts in state and reward formulation. Intersection Agents within each region \mathcal{R}_k share a single DDQN policy, but both the state and reward fed to the regional agent u_k are strictly local and use the same definition of state and reward local components employed in our implementations of SEMI-CTDE, OneHop and RegionWide

models:

$$s_i = s_i^{\text{local}}, \quad r_i = r_i^{\text{local}}, \quad \forall i \in \mathcal{R}_k, \quad (35)$$

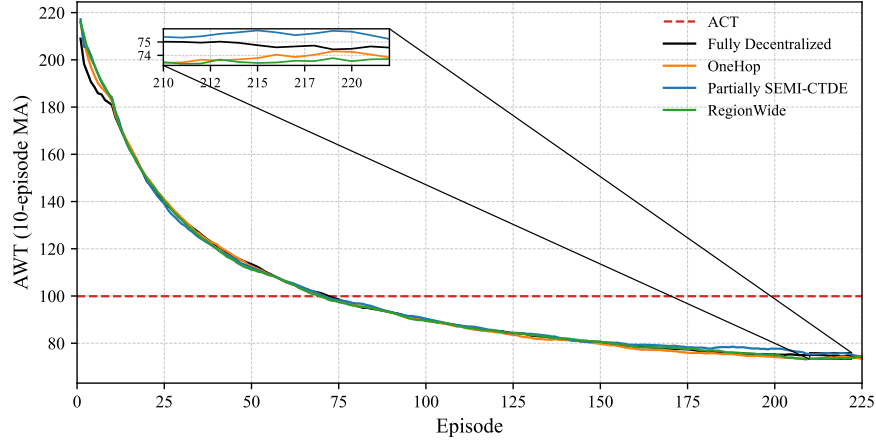
which is equivalent to setting regional weights to zero. Network partitioning follows the same region definitions used throughout this work.

6.3. Results

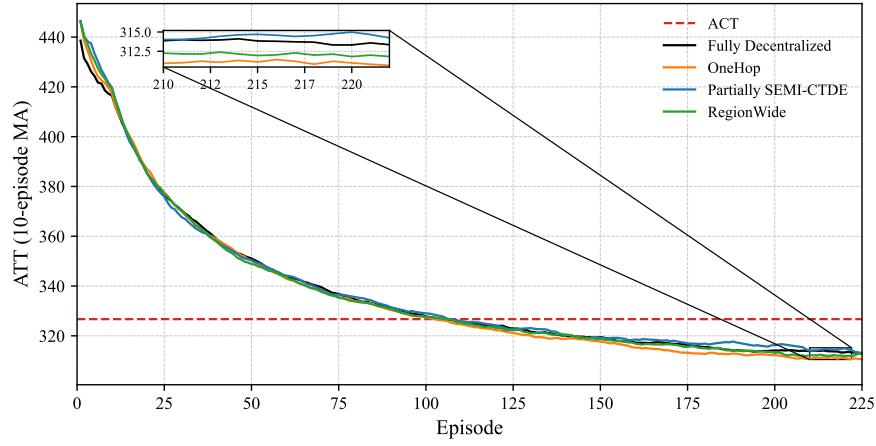
Training behavior: Figure 8 tracks the evolution of network-wide AWT and ATT during training on the uniform-demand setting (U1). All learning-based policies improve steadily; curves descend and then stabilize as exploration decays. For ATT, Partially SEMI-CTDE exhibits an early advantage between Episodes 25–40—likely due to its smaller, simpler state and reward definitions—yet from roughly Episode 100 onward OneHop consistently dominates and maintains a clear margin through the end of training; RegionWide is the second-best performer and, after convergence, opens a clear gap over both Fully Decentralized and Partially SEMI-CTDE. For AWT, Partially SEMI-CTDE again leads in the early stages, but from around Episode 120 OneHop becomes dominant; after Episode 200, RegionWide surpasses OneHop, and both maintain a pronounced margin over the other two baselines. A consistent observation is that Fully Decentralized outperforms Partially SEMI-CTDE on both metrics: because they share identical local state and reward while Fully Decentralized trains a separate network per intersection (greater parameter capacity), Partially SEMI-CTDE’s parameter sharing reduces capacity without adding regional terms, indicating that parameter sharing alone does not guarantee gains and that state/reward design is equally critical. As is visible in both metrics, the SEMI-CTDE models (RegionWide, OneHop) outperform the other algorithms, and this corroborates that regional state/reward alongside coordination via parameter sharing improves learning.

Test-time performance: To better analyze and compare the results, we group the tests based on the intensity of the arrival distributions. To ensure robustness, each model is tested 10 times with different random seeds for each flow. We report the mean and standard deviation of the model performance in AQL and AWT (Tables 5–8).

Under light-demand arrival distributions (Tables 5–6), OneHop consistently achieves the lowest average queues and waiting times among all models. This is expected because, in these distributions, congestion is mild, queues remain short, and interactions are dominated by the immediate upstream and downstream neighbors of each intersection rather than by far-away parts of the region. OneHop’s bounded neighborhood design exposes exactly this local coupling: the regional terms summarize only the immediate influential vicinity, so the regional agent receives just enough information to coordinate adjacent intersection agents efficiently without being distracted by weakly relevant fluctuations elsewhere. In contrast, RegionWide aggregates state and reward information over the entire region, mixing lightly



(a) Average Waiting Time (AWT).



(b) Average Travel Time (ATT).

Figure 8: 10-episode moving averages of network-wide average waiting time (AWT) and average travel time (ATT) over 225 episodes, with a zoom on Episodes 210–222.

Table 5
Average Queue Length (AQL) - Light flows

Flow	RegionWide	OneHop	Partially SEMI-CTDE	Fully Decentralized	Actuated
W1	7.67 ± 0.05	6.90 ± 0.04	7.19 ± 0.08	7.60 ± 0.07	7.52
W2	8.01 ± 0.09	7.21 ± 0.02	7.54 ± 0.04	7.91 ± 0.05	8.20
G1	8.46 ± 0.12	7.86 ± 0.10	8.26 ± 0.09	8.52 ± 0.18	8.92

Table 6
Average Waiting Time (AWT) - Light flows

Flow	RegionWide	OneHop	Partially SEMI-CTDE	Fully Decentralized	Actuated
W1	38.35 ± 0.50	28.27 ± 0.22	32.35 ± 0.49	35.73 ± 0.41	34.31
W2	40.36 ± 0.74	30.33 ± 0.20	34.28 ± 0.33	37.12 ± 0.28	38.95
G1	47.38 ± 0.99	38.00 ± 0.65	43.16 ± 0.70	45.17 ± 0.96	50.11

loaded and moderately loaded intersections into a single coarse summary. When flows are light, these whole-region aggregates carry little signal about the few locations where temporary queues actually form, and they can even be misleading by smoothing out localized imbalances that the regional agent should react to. As a result, the learning signal for RegionWide becomes noisy and poorly aligned with the truly critical decisions at each intersection agent, leading to systematically worse AQL and AWT despite using the same network capacity as OneHop. Finally, the light-flow results

also show that Partially SEMI-CTDE consistently outperforms the Fully Decentralized baseline. Both rely purely on local information, but Partially SEMI-CTDE shares a single DDQN per region, so each update is trained on experience collected from multiple similar intersections. This parameter sharing increases sample efficiency, stabilizes learning, and yields smoother, more coherent signal policies across the region, whereas independent learners in the Fully Decentralized setup must each generalize from a much smaller, noisier local experience stream, which hurts their ability to keep

Table 7

Average queue length (AQL) - Heavy flows

Flow	RegionWide	OneHop	Partially SEMI-CTDE	Fully Decentralized	Actuated
W3	11.54 ± 0.16	13.07 ± 0.92	13.59 ± 0.23	12.34 ± 0.14	12.96
W4	13.26 ± 0.19	17.60 ± 1.49	17.21 ± 0.48	117.16 ± 111.39	15.07
G2	10.67 ± 0.17	11.68 ± 0.44	12.15 ± 0.14	11.39 ± 0.29	11.53

queues and delays low even in these relatively easy traffic conditions.

Under heavy-demand arrival distributions (Tables 7–8), RegionWide clearly dominates all other controllers, indicating that whole-region aggregation becomes crucial once congestion intensifies and queues begin to interact across wide spatial scales. In these distributions, bottlenecks no longer arise in isolation: spillback from one intersection can quickly propagate through corridors and across the region, and RegionWide’s design—pooling information over all intersections in the region—gives each regional agent a faithful picture of these global imbalances. This richer regional information allows the regional agent to coordinate actions in a way that proactively protects critical corridors and dissipates queues before they cascade, which is reflected in RegionWide’s consistently superior queues and delays across all heavy flows. The most striking case is W4, the heaviest demand pattern in our tests, where RegionWide not only maintains stable performance but opens a very large margin over all other learning-based methods, demonstrating strong generalization under extreme arrivals. In contrast, OneHop performs poorly in these distributions: its bounded neighborhood regional terms, which were ideal under light flows, become insufficient once congestion and spillback span multiple intersections, so the regional agent reacts shortsightedly to local symptoms rather than the region-scale structure of queues. Nevertheless, OneHop still outperforms Partially SEMI-CTDE, which lacks regional information altogether and therefore cannot exploit any cross-intersection coordination, underscoring that even limited regional state can be helpful when combined with parameter sharing. Fully Decentralized exhibits an interesting trade-off: in most heavy flows where it runs, its larger parameter capacity (a separate DDQN per intersection) yields slightly better performance than OneHop, suggesting that, in the absence of strong regional signals, sheer model capacity can partially compensate. However, in W4 the Fully Decentralized model fails entirely to mitigate traffic congestion, whereas other algorithms remain stable and effective, reinforcing the importance of region-based design and shared parameters for robustness under extreme congestion. Finally, the actuated baseline is consistently outperformed by all learning-based models. In heavy flows, the gap in AWT and AQL becomes substantial, but even in light flows the learning-based policies retain a smaller yet persistent advantage, indicating that data-driven coordination yields meaningful gains over traditional detector-based control across the whole range of arrival distributions.

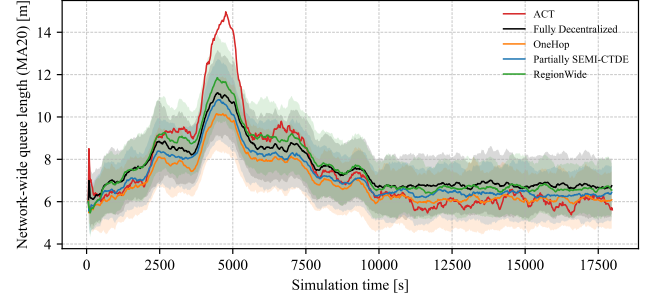
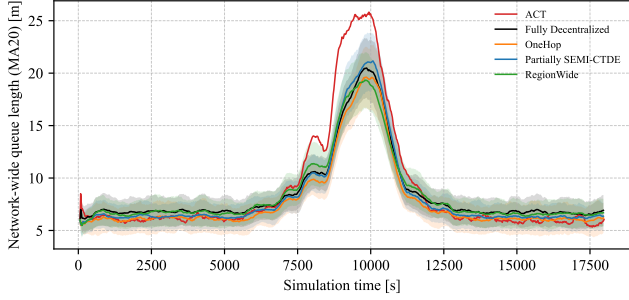
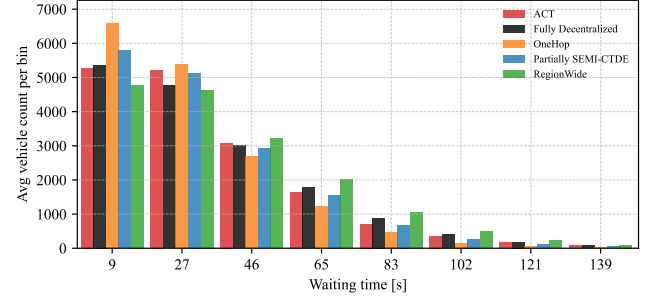
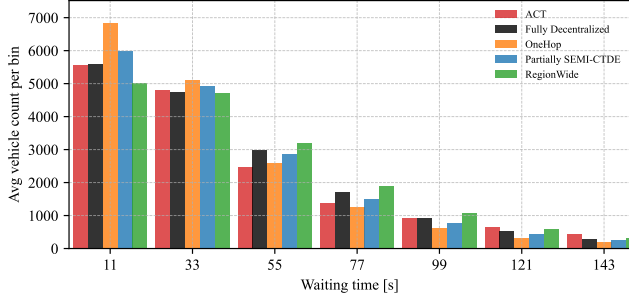
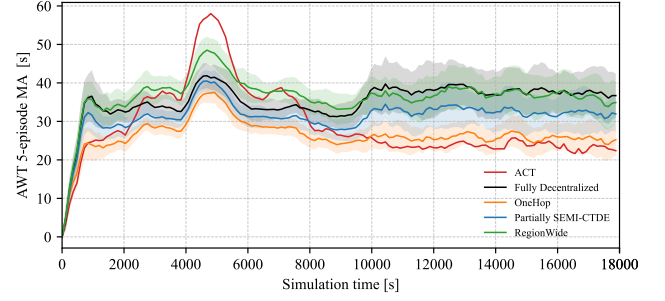
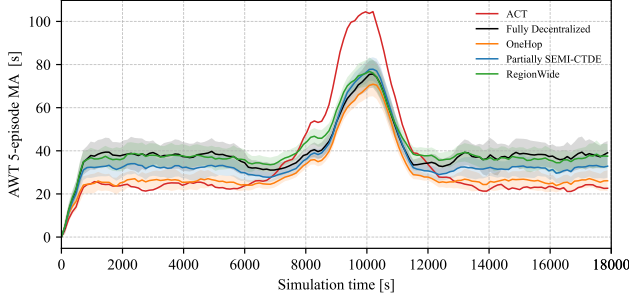
Table 8

Average Waiting Time (AWT) - Heavy flows

Flow	RegionWide	OneHop	Partially SEMI-CTDE	Fully Decentralized	Actuated
W3	65.38 ± 1.22	67.61 ± 3.19	72.91 ± 0.98	66.85 ± 0.92	76.05
W4	75.99 ± 1.51	95.48 ± 8.03	94.11 ± 3.54	400.42 ± 213.56	91.33
G2	65.92 ± 0.94	67.65 ± 2.96	72.34 ± 1.02	67.93 ± 1.97	74.80

To complement the aggregate, episode-level statistics reported in Tables 5–8, we next examine how network performance evolves over simulation time within representative frozen test episodes drawn from the very same runs used to compute these tables. Instead of summarizing each run by a single scalar, these plots track the trajectories of AQL and AWT. This temporal perspectives along with waiting time histograms (Figures 9–10) reveals how each model responds to demand peaks, how it recovers from it and lets us compare their performances during different arrival rates, thereby providing a more fine-grained view of the mechanisms underlying the performance gaps observed in the tables.

For the light-demand flows (G1, W1), the temporal plots and waiting-time histograms reinforce the same hypothesis as the aggregate tables while revealing more detail about how each model behaves over a full episode. In the Gaussian flow G1, OneHop clearly dominates the other learning-based models in both AQL and AWT traces: it keeps queues and delays lowest not only around the peak but also in the lower-demand periods before and after, indicating that its bounded-neighborhood regional information is exactly tuned to the spatial scale of interactions in these light arrival distributions. The actuated model, by contrast, performs particularly poorly during the peak, with pronounced spikes in both AWT and AQL, which explains its consistently inferior episode-level averages; however, its trajectories before and after the peak are slightly better than OneHop, suggesting that a simple rule-based strategy can still be competitive when arrival rates are very low. In G1, Partially SEMI-CTDE maintains lower queues and waiting times than both Fully Decentralized and RegionWide in the off-peak periods, in line with the table results and confirming that regional parameter sharing improves sample efficiency even when only local information is used. Around the peak, these three models show broadly similar behavior, all lagging behind OneHop, but the AQL curves reveal that RegionWide starts to close the gap and can even slightly surpass OneHop in the very center of the Gaussian peak, hinting that whole-region aggregation becomes more helpful once instantaneous arrival approaches heavier rates. The Weibull flow W1 mirrors most of these patterns with a key difference at peak: OneHop again yields the lowest queues and waiting times and actuated again performs worst, but now RegionWide is clearly inferior to both Fully Decentralized and Partially SEMI-CTDE at the peak. This can be explained by the fact that the peak in G1 is more intense than the peak in W1, confirming that it is only under genuinely heavier arrivals



(a) Flow G1

(b) Flow W1

Figure 9: Intra episode performance across light arrivals.

that whole-region summaries inject useful, relevant information that improves the model’s decision making. Finally, the waiting-time histograms for both G1 and W1 show that OneHop concentrates a much larger fraction of vehicles in the low-wait bins, with markedly fewer vehicles suffering long delays, whereas the other models exhibit heavier tails. This distributional view confirms that OneHop not only improves average performance but also delivers a better individual driving experience by reducing the likelihood of vehicles experiencing prolonged waiting times.

For the heavy-demand flows (G2, W3), the temporal plots again refine and support the aggregate picture from the tables, while clarifying when and why each model succeeds or fails. In the Gaussian flow G2, the AWT curves show that before the peak both OneHop and the actuated models maintain the lowest delays, consistent with our earlier observation that OneHop is well suited to moderate arrivals and that a simple rule-based strategy can be competitive at low demand. In pre-peak arrivals, Partially SEMI-CTDE tracks these two reasonably well and clearly outperforms both Fully Decentralized and RegionWide, as expected from

its parameter sharing and purely local information. Around the peak, however, the ordering reverses: RegionWide becomes the clear best performer, keeping AWT lowest, while OneHop, Partially SEMI-CTDE, and actuated all exhibit much higher delays; Fully Decentralized sits in between, worse than RegionWide but better than other three, likely because its larger number of learnable parameters grants it stronger representational capacity in the high-demand arrival rates. The most striking behavior occurs after the peak: Partially SEMI-CTDE and Fully Decentralized are unable to discharge the accumulated congestion and their AWT and AQL curves remain high and even become worse, whereas OneHop and actuated recover quickly and achieve the best post-peak performance, with RegionWide trailing slightly behind them. This pattern suggests that the strong advantage of RegionWide in the episode-level metrics comes primarily from its ability to manage the peak itself; outside the peak it is not the best performer, but its superior control during the most congested period dominates the aggregate outcome. The AQL trajectories for G2 follow a similar pattern: RegionWide dominates at the peak, the gap to OneHop narrows after the peak, and OneHop and Partially SEMI-CTDE

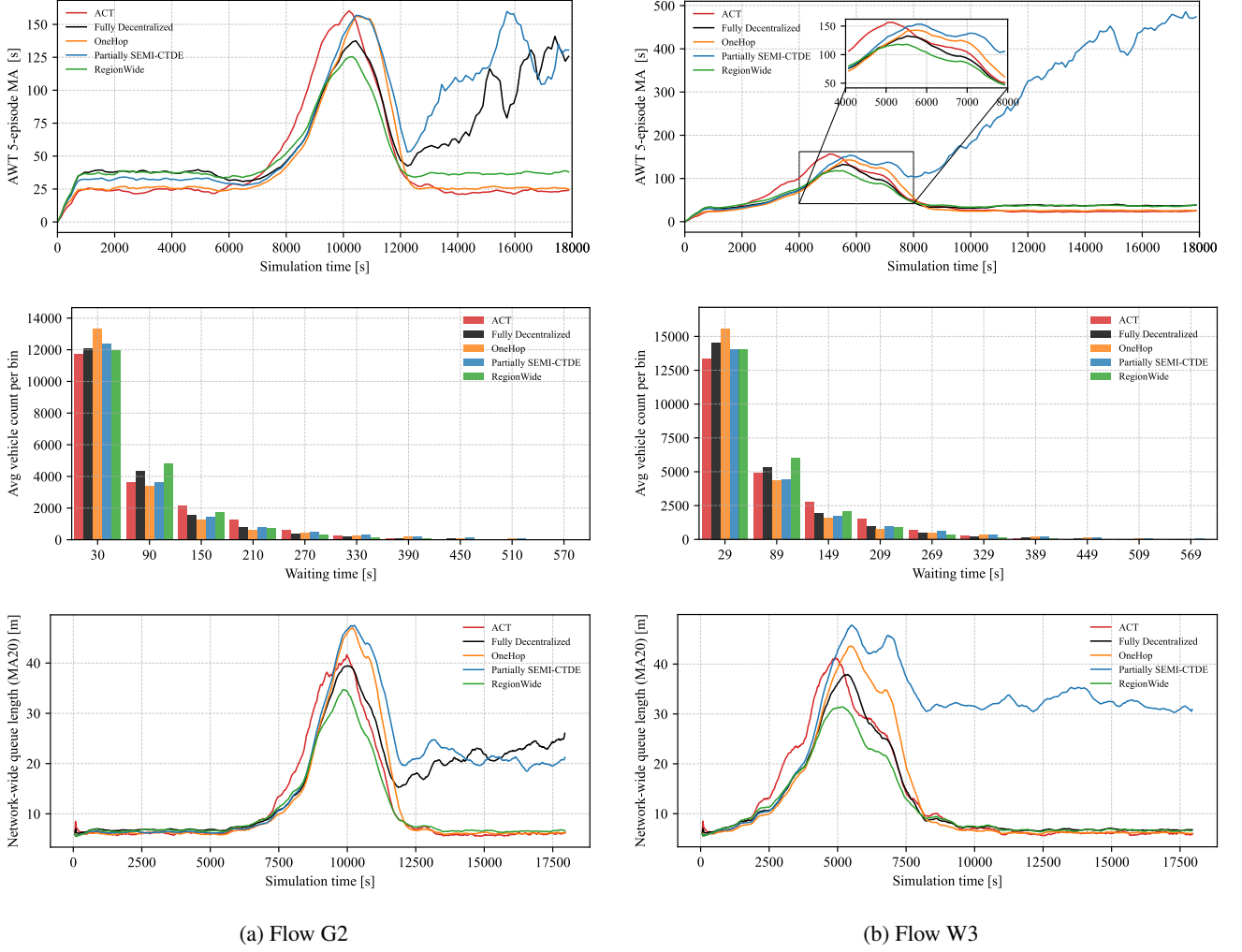


Figure 10: Intra episode performance across heavy arrivals.

can even fall below actuated when regional information is absent, underscoring that in genuinely heavy demand the presence and scale of regional information are critical. In W3, the qualitative picture remains the same: RegionWide again dominates at the peak, and OneHop together with actuated provide the best recovery after the peak, but here only Partially SEMI-CTDE fails to fully recover while Fully Decentralized manages to discharge more effectively than in G2, with all other relative comparisons preserved. The waiting-time histograms for G2 and W3 further clarify these effects: the lowest waiting-time bin is dominated by OneHop, with actuated contributing the smallest fraction there, which aligns with our conclusion that OneHop is particularly well suited for lower and moderate arrival rates. The second bin is dominated by RegionWide, reflecting its behavior at peak: during the heaviest intervals, RegionWide is essentially the only model that keeps network-wide delays at a moderate and manageable level rather than allowing them to explode, so many vehicles accumulate in this intermediate waiting range. In subsequent bins corresponding to larger waiting times, RegionWide exhibits the lowest frequencies among all learning-based policies, confirming that under

heavy flows it not only controls peak congestion more effectively but also substantially reduces the probability of very long individual delays.

Taken together, our detailed, multi-perspective analysis—spanning aggregate episode metrics, stepwise temporal profiles, and waiting-time distributions—shows that SEMI-CTDE with carefully designed regional information delivers robust improvements across a wide range of traffic configurations. OneHop is the most effective in light and moderately loaded regimes, where bounded-neighborhood summaries anchor just the right level of coordination, while RegionWide is the best choice under heavy congestion, where whole-region aggregation is needed to manage spillback and prevent collapse. These all confirm the value of regional parameter sharing, which highlights that region-centric semi-centralized learning is key to achieving superior network efficiency and less intense delay distributions.

7. Conclusion

In this work, we formulated urban traffic signal control as a region-based multi-agent reinforcement learning problem and introduced *SEMI-CTDE* architecture, a semi-centralized training, decentralized execution approach tailored to this setting. Beyond this, we provided a self-contained problem formulation for region-based MARL in TSC, explicitly formalizing regions, intersection agents, and regional agents together with their associated decision processes, composite state space and reward functions designed specifically to operate in region based environments. To the best of our knowledge, this is the first work to articulate these components within a unified region-centric paradigm, which can serve as a reusable foundation for subsequent research on coordinated traffic signal control. To obtain regions, we employed a fuzzy-graph α -cut method to extract regions whose intersections are tightly coupled in terms of traffic features, thereby aligning the learning architecture with the dominant flow dependencies in the network. The overall architecture combines topology and location-aware encoders, admissibility-aware action mapping, asynchronous event-driven experience gathering, and regional parameter sharing via DDQN-based agents, enabling semi-centralized learning at region scope with fully decentralized execution. We instantiated this architecture with two concrete models, *RegionWide* and *OneHop*, that share all *SEMI-CTDE* backbones and differ only in the receptive field used for their regional components: whole-region summaries in *RegionWide* versus bounded one-hop neighborhoods in *OneHop*.

Comprehensive experiments on the 5×5 grid network under Gaussian and Weibull arrival distributions, structured around targeted comparisons, examined (i) the importance of composite local–regional state and reward design, (ii) the effect of regional parameter sharing against a fully decentralized baseline. The results closely align with the main ideas behind *SEMI-CTDE*: grouping tightly coupled intersections into regions and coupling this regioning with composite state and reward formulations yields consistently superior performance compared with purely local learning and conventional rule-based control. The results further revealed a clear relation between receptive-field choice and arrival flow demand: *OneHop* is most effective under light and moderately demanded flows while *RegionWide* dominates under heavy flows. Together, these findings highlight that region-centric semi-centralized learning combined with carefully structured state and reward designs yields robust, interpretable gains over both purely local learning and traditional rule-based control.

Despite these contributions, our study has several limitations that suggest avenues for future work. First, the implemented models consider a restricted discrete action space built from four phase logics with short/long durations; more complex phasing schemes, as well as continuously variable green durations, are not explored here even though *SEMI-CTDE* itself can naturally accommodate them. Second, our

state design relies on hand-crafted spatial and temporal aggregates; while this yields interpretability, it may underutilize the expressive power of modern deep models. A natural extension is to integrate learned feature extractors—such as graph neural networks to capture finer-grained spatial structure over the road network and LSTM- or other sequence models to encode temporal dynamics—within the *SEMI-CTDE* backbone, replacing or augmenting the manually designed blocks. Exploring these richer architectures, together with more general action parameterizations and larger-scale or real-world networks, forms a promising direction for future research on region-based multi-agent traffic signal control under the *SEMI-CTDE* paradigm.

References

- Abdoos, M., 2021. Fuzzy graph and collective multiagent reinforcement learning for traffic signals control. *IEEE Intelligent Systems* 36, 48–55. doi:10.1109/MIS.2020.3000180.
- Abdoos, M., Mozayani, N., Bazzan, A.L.C., 2011. Traffic light control in non-stationary environments based on multi agent q-learning, in: 2011 14th International IEEE Conference on Intelligent Transportation Systems (ITSC), pp. 1580–1585. doi:10.1109/ITSC.2011.6083114.
- Abdulhai, B., Pringle, R., Karakoulas, G.J., 2003. Reinforcement learning for true adaptive traffic signal control. *Journal of Transportation Engineering* 129, 278–285. doi:10.1061/(ASCE)0733-947X(2003)129:3(278).
- Ault, J., Hanna, J.P., Sharon, G., 2020. Learning an interpretable traffic signal control policy, in: Proceedings of the 19th International Conference on Autonomous Agents and Multiagent Systems (AAMAS 2020), p. 88–96. doi:10.5555/3407923.3407957.
- Bao, J., Wu, C., Lin, Y., Zhong, L., Chen, X., Yin, R., 2023. A scalable approach to optimize traffic signal control with federated reinforcement learning. *Scientific Reports* 13, 19184. doi:10.1038/s41598-023-46074-3.
- Bie, Y., Ji, Y., Ma, D., 2024. Multi-agent deep reinforcement learning collaborative traffic signal control method considering intersection heterogeneity. *Transportation Research Part C: Emerging Technologies* 164, 104663. URL: <https://www.sciencedirect.com/science/article/pii/S0968090X24001840>, doi:https://doi.org/10.1016/j.trc.2024.104663.
- Bouktif, S., Cheniki, A., Ouni, A., El-Sayed, H., 2023. Deep reinforcement learning for traffic signal control with consistent state and reward design approach. *Knowledge-Based Systems* 267, 110440. doi:10.1016/j.knsys.2023.110440.
- Cai, S., Fang, J., Xu, M., 2025. Xlight: An interpretable multi-agent reinforcement learning approach for traffic signal control. *Expert Systems with Applications* 273, 126938. URL: <https://www.sciencedirect.com/science/article/pii/S0957417425005603>, doi:https://doi.org/10.1016/j.eswa.2025.126938.
- Casas, N., 2017. Deep deterministic policy gradient for urban traffic light control. *arXiv preprint arXiv:1703.09035*.
- Chu, T., Wang, J., Codecà, L., Li, Z., 2020. Multi-agent deep reinforcement learning for large-scale traffic signal control. *IEEE Transactions on Intelligent Transportation Systems* 21, 1086–1095. doi:10.1109/TITS.2019.2901791.
- Gu, H., Wang, S., Jia, D., Zhang, Y., Luo, Y., Mao, G., Wang, J., Gee Lim, E., 2025. Communication strategy on macro-and-micro traffic state in cooperative deep reinforcement learning for regional traffic signal control. *IEEE Transactions on Intelligent Transportation Systems* 26, 12183–12196. doi:10.1109/TITS.2025.3556931.
- Gu, H., Wang, S., Ma, X., Jia, D., Mao, G., Lim, E.G., Wong, C.P.R., 2024. Large-scale traffic signal control using constrained network partition and adaptive deep reinforcement learning. *IEEE Transactions on Intelligent Transportation Systems* 25, 7619–7632. doi:10.1109/TITS.2024.3352446.
- van Hasselt, H., Guez, A., Silver, D., 2016. Deep reinforcement learning with double q-learning, in: Proceedings of the Thirtieth AAAI Conference on Artificial Intelligence (AAAI 2016), pp. 2094–2100. doi:10.5555/3016100.3016191.

- Hu, K., Li, M., Song, Z., Xu, K., Xia, Q., Sun, N., Zhou, P., Xia, M., 2024. A review of research on reinforcement learning algorithms for multi-agents. *Neurocomputing* 599, 128068. URL: <https://www.sciencedirect.com/science/article/pii/S0925231224008397>, doi:<https://doi.org/10.1016/j.neucom.2024.128068>.
- INRIX, . INRIX 2024 Global Traffic Scorecard. Tech. Rep.. INRIX. URL: <https://inrix.com/scorecard/>.
- Li, M., Pan, X., Liu, C., Li, Z., 2025. Federated deep reinforcement learning-based urban traffic signal optimal control. *Scientific Reports* 15, 11724. doi:[10.1038/s41598-025-91966-1](https://doi.org/10.1038/s41598-025-91966-1).
- Li, Y., Zhang, Y., Li, X., Sun, C., 2024. Regional multi-agent cooperative reinforcement learning for city-level traffic grid signal control. *IEEE/CAA Journal of Automatica Sinica* 11, 1987–1998. doi:[10.1109/JAS.2024.124365](https://doi.org/10.1109/JAS.2024.124365).
- Liang, X., Du, X., Wang, G., Han, Z., 2019. A deep reinforcement learning network for traffic light cycle control. *IEEE Transactions on Vehicular Technology* 68, 1243–1253. doi:[10.1109/TVT.2018.2890726](https://doi.org/10.1109/TVT.2018.2890726).
- Liu, B., Ding, Z., 2022. A distributed deep reinforcement learning method for traffic light control. *Neurocomputing* 490, 390–399. URL: <https://www.sciencedirect.com/science/article/pii/S092523122101818X>, doi:<https://doi.org/10.1016/j.neucom.2021.11.106>.
- Liu, B., Liu, X., Chen, C., Huang, J., Ding, Z., 2025. Decentralized neighboring information fusion for traffic network signal control. *Neurocomputing* 650, 130834. URL: <https://www.sciencedirect.com/science/article/pii/S0925231225015061>, doi:<https://doi.org/10.1016/j.neucom.2025.130834>.
- Lopez, P.A., Behrisch, M., Bieker-Walz, L., Erdmann, J., Flötteröd, Y.P., Hilbrich, R., Lücken, L., Rummel, J., Wagner, P., Wießner, E., 2018. Microscopic traffic simulation using sumo, in: *The 21st IEEE International Conference on Intelligent Transportation Systems*, IEEE. URL: <https://elib.dlr.de/124092/>.
- Lu, Y., Li, C., Yu, H., Wang, H., 2025. Soft actor-critic based regional traffic signal control in connected environment and its application in priority signal control. *Journal of Intelligent Transportation Systems* URL: <https://www.sciencedirect.com/science/article/pii/S1547245025000325>, doi:<https://doi.org/10.1080/15472450.2025.2532724>.
- Mnih, V., Kavukcuoglu, K., Silver, D., Rusu, A.A., Veness, J., Bellemare, M.G., Graves, A., Riedmiller, M., Fidjeland, A.K., Ostrovski, G., Petersen, S., Beattie, C., Sadik, A., Antonoglou, I., King, H., Kumaran, D., Wierstra, D., Legg, S., Hassabis, D., 2015. Human-level control through deep reinforcement learning. *Nature* 518, 529–533. doi:[10.1038/nature14236](https://doi.org/10.1038/nature14236).
- Noaen, M., Naik, A., Goodman, L., Crebo, J., Abrar, T., Abad, Z., Bazzan, A., Far, B., 2022. Reinforcement learning in urban network traffic signal control: A systematic literature review. *Expert Systems with Applications* 199, 116830. doi:[10.1016/j.eswa.2022.116830](https://doi.org/10.1016/j.eswa.2022.116830).
- Rasheed, F., Yau, K., Noor, R.M., Wu, C., Low, Y.C., 2020. Deep reinforcement learning for traffic signal control: A review. *IEEE Access* 8, 208016–208044. doi:[10.1109/ACCESS.2020.3034141](https://doi.org/10.1109/ACCESS.2020.3034141).
- Ren, F., Dong, W., Zhao, X., Zhang, F., Kong, Y., Yang, Q., 2024. Two-layer coordinated reinforcement learning for traffic signal control in traffic network. *Expert Systems with Applications* 235, 121111. URL: <https://www.sciencedirect.com/science/article/pii/S0957417423016135>, doi:<https://doi.org/10.1016/j.eswa.2023.121111>.
- Saadi, A., Abghour, N., Chiba, Z., Moussaid, K., Ali, S., 2025. A survey of reinforcement and deep reinforcement learning for coordination in intelligent traffic light control. *Journal of Big Data* 12, 84. URL: <https://journalofbigdata.springeropen.com/articles/10.1186/s40537-025-01104-x>, doi:[10.1186/s40537-025-01104-x](https://doi.org/10.1186/s40537-025-01104-x).
- Saeedmanesh, M., Geroliminis, N., 2016. Clustering of heterogeneous networks with directional flows based on “snake” similarities. *Transportation Research Part B: Methodological* 91, 250–269. URL: <https://www.sciencedirect.com/science/article/pii/S0191261515302605>, doi:<https://doi.org/10.1016/j.trb.2016.05.008>.
- Song, X.B., Zhou, B., Ma, D., 2024. Cooperative traffic signal control through a counterfactual multi-agent deep actor critic approach. *Transportation Research Part C: Emerging Technologies* 160, 104528. URL: <https://www.sciencedirect.com/science/article/pii/S0968090X24000494>, doi:<https://doi.org/10.1016/j.trc.2024.104528>.
- Spall, J.C., 1992. Multivariate stochastic approximation using a simultaneous perturbation gradient approximation. *IEEE Transactions on Automatic Control* 37, 332–341. doi:[10.1109/9.119632](https://doi.org/10.1109/9.119632).
- Sutton, R.S., Barto, A.G., 2018. *Reinforcement Learning: An Introduction*. 2 ed., MIT Press, Cambridge, MA.
- Tan, T., Bao, F., Deng, Y., Jin, A., Dai, Q., Wang, J., 2020. Cooperative deep reinforcement learning for large-scale traffic grid signal control. *IEEE Transactions on Cybernetics* 50, 2687–2700. doi:[10.1109/TCYB.2019.2904742](https://doi.org/10.1109/TCYB.2019.2904742).
- Wang, T., Zhu, Z., Zhang, J., Tian, J., Zhang, W., 2024. A large-scale traffic signal control algorithm based on multi-layer graph deep reinforcement learning. *Transportation Research Part C: Emerging Technologies* 162, 104582. URL: <https://www.sciencedirect.com/science/article/pii/S0968090X24001037>, doi:<https://doi.org/10.1016/j.trc.2024.104582>.
- Watkins, C.J.C.H., Dayan, P., 1992. Q-learning. *Machine Learning* 8, 279–292. doi:[10.1007/BF00992698](https://doi.org/10.1007/BF00992698).
- Wu, T., Zhou, P., Liu, K., Yuan, Y., Wang, X., Huang, H., Wu, D.O., 2020. Multi-agent deep reinforcement learning for urban traffic light control in vehicular networks. *IEEE Transactions on Vehicular Technology* 69, 8243–8256. doi:[10.1109/TVT.2020.2997896](https://doi.org/10.1109/TVT.2020.2997896).
- Xing, Y., Li, W., Liu, W., Li, Y., Zhang, Z., 2022. A dynamic regional partitioning method for active traffic control. *Sustainability* 14. URL: <https://www.mdpi.com/2071-1050/14/16/9802>, doi:[10.3390/su14169802](https://doi.org/10.3390/su14169802).
- Yau, K.L.A., Qadir, J., Khoo, H.L., Ling, M.H., Komisaruk, P., 2017. A survey on reinforcement learning models and algorithms for traffic signal control. *ACM Computing Surveys* 50. doi:[10.1145/3068287](https://doi.org/10.1145/3068287).
- Yi, C., Wu, J., Ren, Y., Ran, Y., Lou, Y., 2022. A spatial-temporal deep reinforcement learning model for large-scale centralized traffic signal control, in: *2022 IEEE 25th International Conference on Intelligent Transportation Systems (ITSC)*, pp. 275–280. doi:[10.1109/ITSC55140.2022.9922459](https://doi.org/10.1109/ITSC55140.2022.9922459).
- Zhao, H., et al., 2024. A survey on deep reinforcement learning approaches for traffic signal control. *Expert Systems with Applications* 234, 119186. doi:[10.1016/j.eswa.2024.2586](https://doi.org/10.1016/j.eswa.2024.2586).